Three-point bending tests of single nanofibers over silicon microstructures

Tesis de post-grado para el grado de
Magíster en Ciencias, mención Física
Departamento de Física, Universidad Técnica
Federico Santa María, Chile.
Valparaíso, 2023

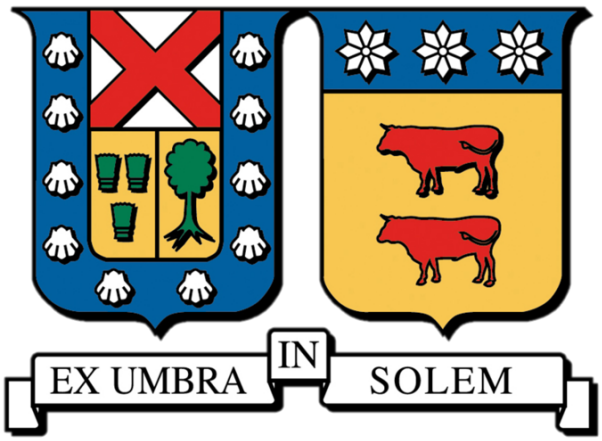

Thesis wrote by:
Benjamín Schleyer Thiers
born in Temuco, Chile.

Advisor	:	Dr. Tomas P. Corrales
Co-Advisor	:	Dr. Yusser Olguín
Committee	:	Dra. Ilka Hermes
		Dra. Valeria del Campo

CONSTANCIA DE VALIDACIÓN Y CONFIDENCIALIDAD DE MONOGRAFÍA A REPOSITORIO ACADÉMICO

1.- IDENTIFICACIÓN DEL TRABAJO ACADÉMICO

Tipo de monografía (marcar una opción): ☐ Memoria o trabajo de título; ☒ Tesis de Postgrado;

Título del trabajo: Three-point bending tests of single nanofibers over silicon microstructures

Nombre del candidato(a): Benjamín Schleyer Thiers

Carrera / Grado: Magíster en Ciencias, mención Física

Campus: Casa Central Valparaiso **;** **Departamento**: Física

2.- VALIDACIÓN DEL PROFESOR GUÍA/DIRECTOR DE TESIS

Yo, Tomas Patricio Corrales Iturriaga, en mi calidad de profesor(a) guía/director(a) del trabajo académico mencionado anteriormente **DEJO CONSTANCIA** que:

- He revisado esta versión del documento y corresponde a la versión final aprobada del trabajo.
- El trabajo cumple con los requisitos académicos y de formato establecidos por la institución

3.- EVALUACIÓN DE CONFIDENCIALIDAD POR PROPIEDAD INDUSTRIAL

☒ El trabajo **NO contiene información que amerite confidencialidad** y puede ser publicado de inmediato en repositorio con acceso abierto.

☐ El trabajo **CONTIENE** información con potenciales implicancias de propiedad industrial o intelectual y requiere un periodo de confidencialidad (embargo) por:

☐ 6 meses; ☐ 12 meses; ☐ 2 años; ☐ 3 años; ☐ 5 años; ☐ 10 años

Fundamentación de la necesidad de confidencialidad (obligatorio si se solicita embargo):

4.- FIRMAS

Profesor(a) guía o director(a) de memoria o tesis:

Fecha: 09/08/25 ; **Firma:** _____

Estudiante o Candidato(a):

Fecha: 09/08/25 ; **Firma:** _____

Este formulario debe ser insertado como página 2 de la memoria o tesis, completado y firmado por estudiante y profesor(a) antes de la entrega en portal PRISMA de Biblioteca USM.

This research was developed between 2023 April and 2025 March, under the guidance of Prof. Dr. Tomas P. Corrales in the physics department of Universidad Técnica Federico Santa María, Valparaíso, Chile

Do or do not, there is no try
-Master Yoda

Agradecimientos

Me gustaría comenzar por agradecer a mi familia, mis padres Juan y Karin, quienes me dieron todo lo que siempre necesité para formar mi propio camino, y avanzar con seguridad hacia mi futuro. No podría describir lo mucho que agradezco la paciencia con la que me educaron y el entusiasmo con el que me enseñaron todos los días de mi vida, haciendo de mí un niño feliz. A mis abuelos y abuelas quienes siempre se preocuparon por nosotros, a todos mis tíos y tías, mis primos y primas por darme los mejores recuerdos. A mi hermano, por ser mi mejor amigo toda la vida, darme infinidad de risas y peleas, y estar siempre para mí.

Debo agradecer al Profesor Dr. Tomás P. Corrales por su guía. Estoy muy agradecido de todo lo que he aprendido trabajando con usted, me siento feliz de haberme formado como físico experimental y de haberme topado con un área de estudio que me guste tanto. Desde el comienzo en su grupo de laboratorio me he sentido aceptado e incluso parte de una pequeña familia. A todos mis compañeros del SPMLab por los cálidos saludos, las risas, las discusiones científicas, los aprendizajes y el apoyo en cada paso de mi vida como científico hasta ahora. Un especial agradecimiento para Dragica y DIego, quienes me enseñaron mucho no solo en el laboratiorio sino que también de la vida como profesional y como persona.

Gracias a mis amigos por confiar en mí y darme siempre todo su apoyo, cada uno de ustedes merece el cielo. Gracias a Pablo, Jorge y Nicolás por estar desde el comienzo de mi camino como Físico, a Matías por acompañarme a estudiar tantas horas y a "Delet this" por ser el mejor grupo de amigos de la historia.

Merecen un espacio de agradecimiento mis colegas y compañeros del postgrado en física, de los que siempre he recibido apoyo, enseñanzas y buena disposición en todo momento, la carrera me encanta, pero ustedes fueron los que cementaron mi gusto por querer compartir lo que sé y ayudar al resto.

Finalmente, pero no menos importante, agradecer a Abish (Avita) Lavoz, por las interminables horas de apoyo durante la redacción de esta tesis, por la motivación que me ha dado cuando más lo necesito, por el cariño incondicional a pesar de mis momentos ocupados, lejos o de estrés, por hacer de mí una persona cada vez mejor y por acompañarme en este proceso tan lindo de mi vida.

Agradecer a los fondecyt regular 1211901 "*Multiscale mechanical properties of hygroscopic nanofibers*" y 1240757 "*Evaluation of a microengineering plat-*

form for the development of peripheral nerve substitutes", y al Núcleo Milenio de NanoBioFísica por aportar los fondos para este trabajo.

Abstract

In tissue engineering, the synthesis and characterization of biomaterials enables scaffold property tailoring for enhancing cell growth, viability, differentiation, etc. By using manufacturing methods based on polymeric solutions, the mixture of several biocompatible components allows for the manipulation of certain characteristics of the material. It is possible, by means of the electrospinning technique, to synthesize polymeric scaffolds made of nanofibers mixed with polyvinyl alcohol, chitosan and salmon gelatin. These components will ultimately present certain features that enables cells to proliferate effectively. Mechanical properties of these scaffolds are commonly studied to understand their interaction with the specific cells that they will support, but the characteristics of isolated nanofibers differ from the scaffold.

In this work, the aim is to understand how composition and environmental changes in humidity can alter the mechanical properties of single nanofibers, and how this variation will impact in the scaffold at micro and macro scale. Mechanical characterization will be mainly achieved by AFM force spectroscopy, force mapping, topography imaging and three-point bending of nanofibers at nano scale, which will allow for precise measuring of Young's modulus. Since different scales are being measured, the method to determine the mechanical modulus of scaffolds will correspond to the colloidal probe technique for AFM, which allows for a greater surface contact area. For nanofibers we will mainly use the three-point bending method. Young's modulus will be compared between different humidities, polymeric composition and scale to obtain a full mechanical characterization as well as an insight in how nanofibers scale their properties in fibrous materials.

Contents

Chapter 1

Introduction

Due to various diseases of infectious, genetic, degenerative, or even physical or chemical origin, the current availability of tissues and organs is not sufficient to meet the needs of patients requiring emergency transplants or more specific and difficult to obtain tissues. In this context, tissue engineering is trying to provide, through different methods, biomaterials, active agents, and even physical-chemical stimulus tissue that could address this deficit [28]. In addition, these methods and techniques have the capability to restore damaged tissue in cases where their natural regeneration is hindered.

1.1 Tissue Engineering

Tissue engineering consists mainly in performing a cell culture on a synthetic scaffold that attempts to mimic the extracellular matrix of the specific tissue that is being replaced, enhance or heal. This reduces some of the drawbacks of performing a regular transplant; like reduction of infections [28], reduction of immune reactions to the new tissue [11] and no need for a donor. This area of study contemplates three main topics: Cells, biomaterials, and growth factors (to enhance cell reproduction, maturation, differentiation, etc.). During this investigation, the main subject will be the biomaterial used as a scaffold.

1.1.1 Scaffold

The scaffold is a biomaterial that is used as a canvas or base to carry out the aforementioned works; this is because it generates a support structure or skeleton for the location of cells, allowing them to accelerate the fixation process, and consequently, induce a faster reproduction [22]. Also, scaffolds allow for cell culture in both the case of *in vitro* culture or direct implantation in damaged tissue, so neighboring cells infiltrate in the scaffold and self-heal the tissue. For this to happen successfully, the scaffold must have certain characteristics. Biocompatibility

is sought, which refers to the response and interaction of the biological environment with the material. This response will depend on numerous factors, both biochemical and physical. In addition to biocompatibility, there is the scaffold's capacity to biodegrade [30], [25], while maintaining its biocompatibility [13]. For this research, the physical properties of scaffolds will be explored, and more precisely, their mechanical properties will be further investigated. It is known that, depending on the tissue to be replicated, the mechanical properties of the scaffold must be similar to those of the extracellular matrix of the host [38].

In addition to mechanical properties, the scaffold must present a certain geometry, porosity and rugosity for the cell to recognize, differentiate and allocate in the biomaterial [37]. Electrospinning is a good candidate to achieve this type of morphology for the scaffold, since it produces a net of nano- and micro fibers, allowing for good porosity and space for the cells to infiltrate in the material [42], as well as a fast production method, proving to be scalable for future applications[33].

1.2 Electrospinning

To fabricate polymeric nanofibers by electrospinning, a solution of the polymer and a suitable solvent must first be prepared. The solution is then pushed through a syringe needle, which generates a meniscus at the end of the needle due to the interaction forces (surface tension). A high electric potential is then applied to the syringe, which electrically charges the mixture. This electrostatic interaction will remain in equilibrium as long as both forces: Surface tension of the solution at the meniscus and the internal electrostatic forces, are equal, generating a structure called a Taylor cone [39], [40] (Figure 1.1). As soon as the electrical force is greater than the surface tension of the solution, small "threads" (or jets) of the polymeric solution will form and will be elongated and ejected towards a collector placed in front of the syringe needle. The collector consists of a conductive plate, which also closes the circuit when connected to electrical ground. On the collector, the polymer jet, already dried during the path between the meniscus and the target, is deposited, forming nanofibers of the original polymer dissolved in the solution.

The electrospinning process will continue as long as there is a constant flow of the solution replacing the volume necessary to form the meniscus [34], [27].

1.3 Polymers

Polymers consist of chains of molecules generally made up of carbon (the backbone of the chain) together with elements such as hydrogen, oxygen, nitrogen, etc. Their length depends on the number of N molecules joined together by a

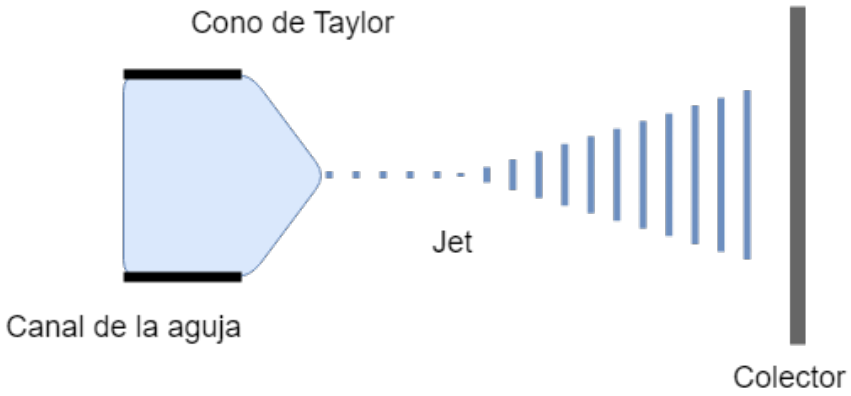

Figure 1.1: *Diagram of Taylor's cone.*

covalent bond. This number of monomeric units is known as the degree of polymerization. The nomenclature of polymers usually depends on the monomer of which they are composed; a very simple example is that of polyethylene (Figure 1.2a), obtained from the polymerization of ethylene. However, there are polymers that do not have a column formed by carbon but are composed of other elements such as silicon, an example of which is PDMS or polydimethylsiloxane.

In this research, we will deal mainly with carbon-based polymers, more specifically polyvinyl alcohol, whose monomer is represented by $[CH_2CH(OH)]$ as shown in Figure 1.2b [2], [16], and which possesses several properties, such as its biocompatibility, can be hydrolyzed to segregate the molecular chains into smaller ones, and is soluble in water. Due to this last characteristic, it is possible to perform various synthesizing and manufacturing techniques [31].

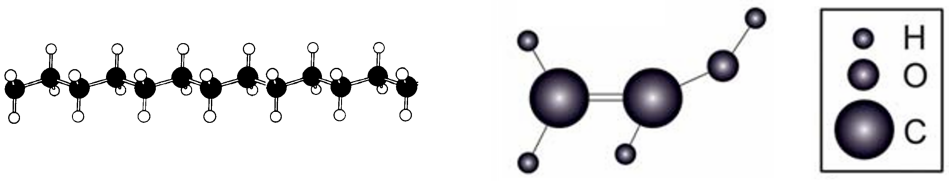

(a) (b)

Figure 1.2: (a)*Polymer example PE, obtained from [31].* (b)*Monomer of Polyvinyl alcohol: Vinyl alcohol structure, obtained from [2].*

Polymers interact with the environment through different external stimuli, e.g., light, temperature, atmospheric pressure, pH, electric field, relative humidity, etc, changing their properties like volume, density, viscosity, stiffness, among others. In this case, the main focus will correspond to analyzing the change of mechanical properties (through Young's modulus "E") in polymeric blended fibers

with humidity (measured in relative humidity RH). This topic was previously studied for PVA nanofibers [24], with the exception that their aim was to study the mmorphological properties of PVA nanofibers under varying humidities and correlate them with their adsorption and mechanical properties using computer simulations.

1.3.1 Synthesis of polymeric nanofibers

The manufacture of polymers is possible due to chemical reactions encompassed in the concept of polymerization. However, the objective was not to synthesize the polymer itself, but rather to produce polymer nanofibers. For this, the electrospinning technique was utilized. This technique will allow us to create nanofibers that after a certain exposure time will form a polymeric membrane [3].

This research focus will be on developing blended polymeric biomaterials combining polyvinyl alcohol (PVA), salmon gelatin (SG), and chitosan (Ch) to create nanofibers with enhanced properties. The PVA/SG/Ch composite has demonstrated promising characteristics including strong cell adhesion, specific differentiation cues for muscle cells, high cell viability, and favorable mechanical properties. The experimental approach involves electrospinning isolated nanofibers by depositing polymer solutions (PVA vs. PVA/SG/Ch blend) onto specialized substrates for 1-30 seconds to achieve suspended fiber configurations. The PVA-only samples will serve as controls to: Establish baseline mechanical behavior under humid conditions, enable direct comparison with the blended polymer's stress response, and isolate the effects of biological components on fiber performance. This dual-strategy methodology allows for systematic evaluation of how synthetic-biological polymer interactions influence the material's mechanical characteristics.

1.4 Atomic Force Microscopy

Atomic force microscopy (AFM) belongs to a group of techniques called scanning probe microscopy (SPM) [6]. This group is characterized by performing a raster scan through a probe, storing a value at each point of a discretized grid according to the resolution of the device. This resolution depends on the type of microscopy performed. For example, in the case of scanning tunneling microscopy (STM), a conductive probe in the form of a tip approaches the surface so that the potential barrier between the two decreases, allowing electrons to tunnel causing a current [5]. This current feedback is the parameter that the system tries to keep constant by means of direct feedback by moving the tip closer or farther away from the sample.

In the case of AFM, a raster scan is performed in the same way as in STM, but in this case the aim is to detect forces of atomic interaction between the tip and the sample. This is possible thanks to a system of cantilever, laser and photo detector, in which the deflection of the beam is measured by the reflection of the laser on it, and is monitored by a photodiode divided into quadrants (Figure 1.3). In this way a laser deflection value is related to the force interacting with the probe. Using this principle, there are different and varied modalities in which measurements can be made, such as force spectroscopy, contact mode (explained above and the first to be developed), non-contact mode, intermittent contact, etc. [9]

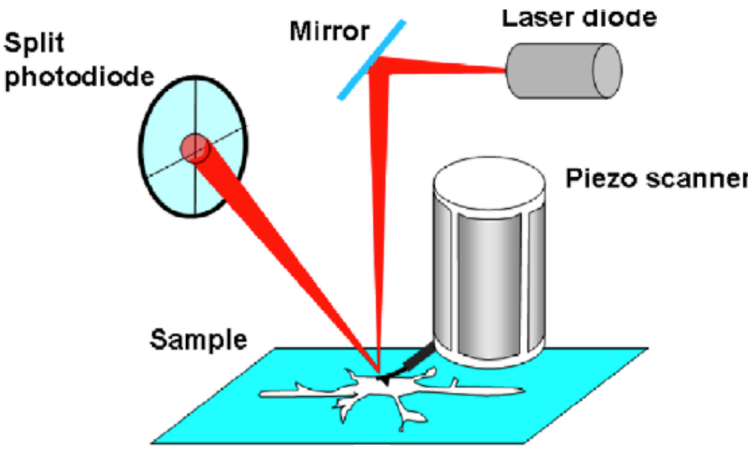

Figure 1.3: *Diagram of cantilever operation by means of a laser and a photo detector divided into quadrants.[1]*

The development of these techniques has contributed to different areas of knowledge since this type of imaging does not have certain restrictions that the predecessors of AFM did, such as the need for a conductive sample in the case of STM, opening the way for the characterization of non-conductive surfaces. Later, with the development of the tapping mode [18], it was possible to analyze samples that did not have the rigidity necessary to perform the conventional contact mode without altering or damaging the sample, i.e., the characterization of biological material, polymers, cells, among others [26], [1]. Due to the fact that in this mode of measurement, the sample is considerably less damaged, almost completely eliminating the dragging that could be caused in the contact mode [9], [1], [18], [26].

In intermittent contact mode, the cantilever behaves like a typical oscillating system, assuming vibrations in the z direction, described as:

$$m\frac{d^2Z(t)}{dt^2} + \gamma_D\frac{dZ(t)}{dt} + kZ(t) = F_0 \sin\omega t \tag{1.1}$$

Where m is the sum of the cantilever and tip mass, γ_D is the damping coefficient and k its elastic constant. Then the resonance frequency is $\omega_0 = \sqrt{k/m}$ and, consequently, its quality factor $Q = \omega_0/\gamma_D$. The equation is satisfied by the solution $Z(t) = Z_0 \sin(\omega t - \phi)$, where Z_0 and ϕ look as shown in Figure 1.4.

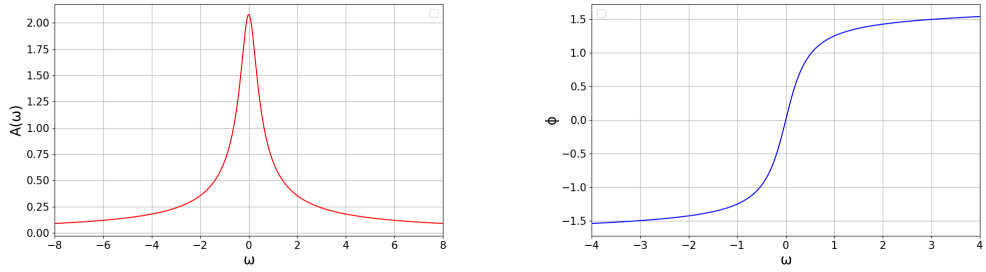

(a) (b)

Figure 1.4: (a)*Solution for the amplitude of the vibrating cantilever.* (b)*Solution for the phase shift of the vibrating cantilever.*

Force Spectroscopy

The very backbone of force measurements are force-distance curves, especially since in AFM it is the main resource obtained from measurements. These curves present different regimes depending on the distance from the substrate. Firstly, far from the surface, no force is sensed (Figure 1.5 I), as the surface of the substrate is approached by the tip, just before entering into contact with the material, an attractive force interacts with it (Figure 1.5 II) making it *snap-in*, finally the tip enters in contact with the substrate (Figure 1.5 III). During the retraction of the cantilever (Figure 1.5 IV), the general interactions are similar, with the main difference that the attractive force, also called the adhesion force, is usually higher than in the approach section. This adhesion is a combined effect of electrostatic interactions, van der Waals force, capillary forces, and forces of chemical origin (acid-base interactions or chemical bonds) [9].

To obtain these curves, it is necessary to determine the sensitivity of the system. Deflection sensitivity refers to the relation between the displacement of the piezoelectric actuator and the voltage induced by the laser reflected over the cantilever on the photodiode, for this a distance force curve is needed as a calibration, typically performed over a hard (non-deformable) substrate, then with the contact regime the sensitivity is obtained through its slope [9].

Finally, spectroscopy can be performed, which records the deflection of the cantilever by sensing the displacement of the laser on the photodiode. With the sensitivity and elastic constant, the obtained values can be converted to force

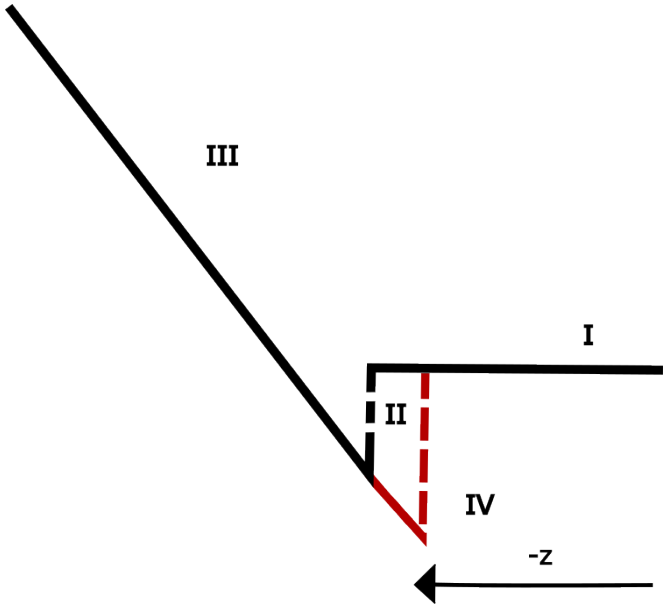

Figure 1.5: *Force versus distance scheme, I: Approach, no interaction (zero force). II: Snap in, attraction forces between the sample and the tip. III: Contact with the substrate, repulsive force and linear deformation. IV: Retraction from the substrate, a higher attraction force is sensed, called adhesion.*

and distance, and the deflection of the cantilever can be decoupled from the total deformation to obtain the deformation of the sample, to fully interpret the data.

Colloidal probe technique

Colloidal probe technique consists of attaching an object in the order of micrometers to the tip of an AFM cantilever to perform force distance measurements similar to the ones performed in usual force spectroscopy, with the advantage of detecting greater adhesion forces, relatively cheap manufacturing, minimizes the apparent surface roughness, since the tip is now orders of magnitude bigger than the standard AFM tip and a known radii to adjust to a contact model for AFM force spectroscopy. Colloidal probes have been used in particle systems with accuracy for a while now, measuring mainly adhesion forces and deformation on surfaces [8]. The production of colloidal probes consists in gluing a colloidal particle, usually spherical, to a tipless cantilever. This process is mostly "homemade", since each experiment requires for a specific particle size [21].

1.5 Mechanical properties

The study of the mechanical properties of a material is one of the most required and common research topics since it allows for the classification and characterization of different materials, according to their strength and deformation. Mechanical properties give us an idea of how the material performs under different contexts. In this case, the main focus will be to understand the response and behavior of the material under mechanical stress, mainly by bending it.

1.5.1 Stress and Strain

Stress and strain are derived by measuring the force applied to a material together with the variation of the length of the material while this force is applied. To properly quantify material stress and strain, it is necessary to define certain concepts for one dimensional systems. First, we understand stress ($sigma$) as the tensile force (F) applied to a material with a cross-sectional area (A) in a plane perpendicular to this force.

$$\sigma = F/A \tag{1.2}$$

Then the relative deformation can be defined as the length variation (Δl) of the material in traction with respect to its initial length (l_0), so we simply represent it by:

$$\epsilon = \Delta l/l_0 \tag{1.3}$$

In the case of three dimensional materials, to fully describe the stress over the system, the stress tensor ($\boldsymbol{\sigma}$) is introduced. Each component of the stress tensor can be defined as the force per unit area over their respective surface (in a specific plane), typically represented with a nine component matrix (as shown in equation 1.4). When the force is applied perpendicularly to a plane, it will be called tensile stress, and it will be represented by the diagonal components of the matrix. In the case where the force is applied parallel to a plane, it will be called sheer stress, corresponding to the six remaining components that are not diagonal.

$$\boldsymbol{\sigma} = \begin{pmatrix} \sigma_{xx} & \sigma_{xy} & \sigma_{xz} \\ \sigma_{yx} & \sigma_{yy} & \sigma_{yz} \\ \sigma_{zx} & \sigma_{zy} & \sigma_{zz} \end{pmatrix} \tag{1.4}$$

As forces are applied to the material, it will suffer deformations depending on the direction of the force applied and the plane in which it is exerted, these deformations, or strain, will be reverted when the force ceases its action as long as the deformations remain within the elastic regime.

The strain tensor ($\boldsymbol{\epsilon}$) can also be represented as a tensor of nine components where its diagonal corresponds to tensile strain (it can be thought of as simple elongations of the material) and the rest of the components to shearing strains of the form:

$$\epsilon_{xy} = \frac{1}{2}\left(\frac{\partial A}{\partial y} + \frac{\partial B}{\partial x}\right) \tag{1.5}$$

$$\epsilon_{yz} = \frac{1}{2}\left(\frac{\partial B}{\partial z} + \frac{\partial C}{\partial y}\right) \tag{1.6}$$

$$\epsilon_{zx} = \frac{1}{2}\left(\frac{\partial A}{\partial z} + \frac{\partial C}{\partial x}\right) \tag{1.7}$$

Taking into account $A(x, y, z)$, $B(x, y, z)$ and $C(x, y, z)$ are components of displacement for x, y and z respectively, and the strain tensor is symmetrical, we could obtain a matrix of the following form to express strain:

$$\boldsymbol{\epsilon} = \begin{pmatrix} \epsilon_{xx} & \epsilon_{yx} & \epsilon_{zx} \\ \epsilon_{yx} & \epsilon_{yy} & \epsilon_{yz} \\ \epsilon_{zx} & \epsilon_{yz} & \epsilon_{zz} \end{pmatrix} \tag{1.8}$$

Then, the total displacement of the material from its original shape ($D(x, y, z)$) will be completely described by the following expression:

$$D(x, y, z) = \boldsymbol{\epsilon} \begin{pmatrix} \Delta x \\ \Delta y \\ \Delta z \end{pmatrix} \tag{1.9}$$

where Δx, Δy and Δz are the displacement variations for each coordinate, then the strain can be interpreted as how much of this displacement actually deformed the material [4],[31].

1.5.2 Young's Modulus

The relationship between stress and relative strain of a material is usually called Young's modulus, which is, in a simplified form, the slope of a stress vs. strain graph. Considering the previously stated concepts, we can write an expression for Young's modulus (E) [41], [7]:

$$E = \sigma/\epsilon = \frac{F}{A}\frac{l_0}{\Delta l} = \frac{F}{\Delta l}\frac{l_0}{A} \tag{1.10}$$

Considering the three dimensional case, the modulus for the material can be described with the components of the corresponding matrix of stress and strain. This value is constant in most cases, since it describes the behavior of the material, normalized by its geometry:

$$E = \frac{\sigma_{ii}}{\epsilon_{ii}} \tag{1.11}$$

Since the material is assumed elastic, the elongation in one axis must produce a contraction in adjacent directions, this is described by another constant related to the material called Poisson's ratio. This constant simply relates strain in the extended and contracted directions as follows:

$$\nu = -\frac{\epsilon_{yy}}{\epsilon_{xx}} \tag{1.12}$$

$$\nu = -\frac{\epsilon_{zz}}{\epsilon_{xx}} \tag{1.13}$$

Considering the x axis as the extending direction. With these two constants, it is possible to describe deformations caused by stress over a material, in the case of longitudinal deformations (the force is applied perpendicular to the plane where the surface is). For shearing deformations, it is necessary to add yet another constant of the material: Shear modulus, described by both Poisson's ratio and Young's modulus, these are related by:

$$G = \frac{E}{2(1+\nu)} \tag{1.14}$$

In this way, the relation between shear strain and shear forces will be as follows:

$$2G = \frac{\sigma_{ij}}{\epsilon_{ij}} \tag{1.15}$$

The shear modulus of materials may vary under some environmental conditions, such as temperature, pressure, electric field, magnetic field, humidity, etc. For this thesis, the main environmental variable will be relative humidity (RH), which is defined as the ratio between the partial pressure of the water vapor (p_{H_2O}) and the vapor pressure in dynamic equilibrium ($p^*_{H_2O}$) at a determined temperature ($RH = p_{H_2O}/p^*_{H_2O}$). Basically, how much pressure of a closed system corresponds to the vapor in relation to the equilibrium pressure for liquid and gaseous water. [7], [31], [4].

1.5.3 Hertz Model

To obtain the mechanical properties of the biomaterials, the primary method will be force spectroscopy through atomic force microscopy (AFM); since the deformation of the material is produced by the AFM tip, it is not trivial to obtain Young's modulus. For this, the model used is the Hertz model, due to its ability to describe the deformation of two spheres (Figure 1.6a) of different radii

and elastic constant, assuming in this case one of the spheres is of infinite radius to act as the sample or substrate (Figure 1.6b).

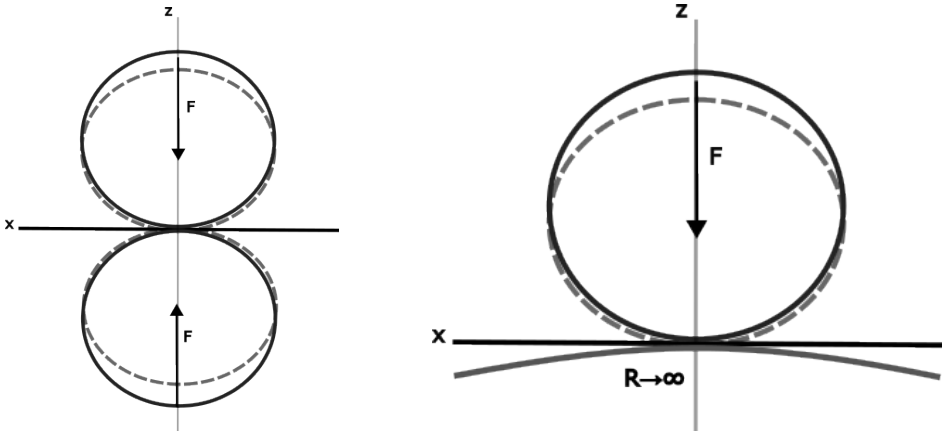

(a) (b)

Figure 1.6: (a)*Scheme of the contact of two spheres, showing the action of the applied force and the deformation after the the contact.* (b)*Scheme of the contact of two spheres as one of the spheres tends its radius to infinite as a simulation of a plane surface.*

Other important assumptions the model makes are that the materials of contacting bodies are homogeneous and isotropic, the loads applied are static, the material is linearly elastic, the contact point is much smaller than the radius of the interacting bodies, there is no friction during the contact and that the deformations are small (infinitesimal strains).

According to the model, when the two surfaces interact with each other, a normal force is applied over them, deforming them into an ellipsoid-like shape (Figure 1.6) [14]. The pressure ($p(r)$) applied to the spheroid is now determined by a relation between its contact surface radius (a) and the radial distance from the center of the contact surface (r):

$$p(r) = p_0 \left(1 - \frac{r^2}{a^2}\right)^{1/2} \tag{1.16}$$

Where p_0 is the pressure on the point $r = 0$ and its value is:

$$p_0 = \frac{3N}{2\pi a^2} \tag{1.17}$$

The contact surface will depend on the elastic constants of the material (K), the force applied to the spheres (N) and the effective radius ($R = 1/R_1 + 1/R_2$), where in the latter case it depends on the radius of both spheres interacting.

$$a = \left(\frac{3NR}{4K}\right)^{1/3} \tag{1.18}$$

Then the constant K is related to the Poisson's ratio and Young's modulus, similarly to the shear modulus:

$$\frac{1}{K} = \frac{(1-\nu_1^2)}{E_1} + \frac{(1-\nu_2^2)}{E_2} \tag{1.19}$$

In this way, the deformation is expressed as follows:

$$\delta = \left(\frac{9N^2}{16RK^2}\right)^{1/3} \tag{1.20}$$

There are some simplifications to these expressions that can be done considering this case (plane substrate), we assume that the second radii is infinite ($R_2 = \infty$), which simplifies the expression for R:

$$\begin{aligned} \frac{1}{R} &= \frac{1}{R_1} + \frac{1}{R_2} \\ R_2 &\to \infty \\ \Rightarrow R &= R_1 \end{aligned}$$

The E modulus of the substrate is considered much higher, so 1.19 simplifies similarly to the previous one [14]:

$$\frac{1}{K} = \frac{(1-\nu_1^2)}{E_1} \tag{1.21}$$

Obtaining a relation between the elastic constant and Poisson's ratio for Young's modulus for a spherical shaped material.

1.5.4 Three-Point Bending

Beam mechanics has been extensively studied since they describe a great portion of materials used by construction, materials science and nano-materials. This research aims to apply it to polymeric nanofibers and describe their mechanical bending properties to better characterize them as a biomaterial for scaffolding and cell culture.

As the material is very thin, we assume that the only stress that contributes is the one in the axial direction of the nanofiber (x axis), then the direction of deformation will be the z direction (Figure 1.7). In this kind of motion, the beam will be stretched and compressed depending on the relative direction of deformation, the side where the beam is convex after applying the force will be

stretching and the side where the beam is concave will be compressing. In the middle will be a line (along the axis of the beam) where the material is neither compressing nor stretching [4].

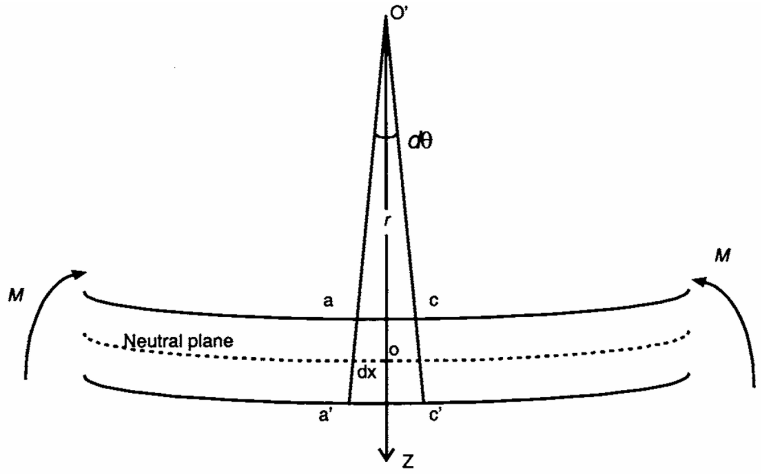

Figure 1.7: *Beam bending diagram [4].*

As the beam deforms, we can define a radii of curvature (r) for an infinitesimal section of the longitudinal axis (dx), this elongation depends on the displacement in the z axis from the equilibrium position. Then the expression for the difference of elongation at different z positions assuming $z = 0$ for the neutral layer (middle) is:

$$\Delta(dx) = (r + z)d\theta - rd\theta = zd\theta \tag{1.22}$$

Then the strain is considered as the relative elongation of a layer with regard to the neutral layer:

$$\epsilon(z) = \frac{z}{r} \tag{1.23}$$

According to equation 1.11 Young's modulus can be described as:

$$E = \frac{\sigma_{xx}}{\epsilon_{xx}} = \frac{\sigma_{xx}r}{z} \tag{1.24}$$

This makes it possible to consider this problem as one-dimensional, due to the beam being very thin, the only stress considered is perpendicular to the plane of cross-sectional area of the fiber.

Mechanical tests in smaller samples have been performed by AFM force spectroscopy, monitoring the deformation of the beam and the cantilever. Usually, the applied technique is called force mapping, a function that allows determining the force distance curves pixel by pixel over a previous topography image,

gaining precision in the beam to test. This approach enables spatially precise characterization of beam bending micro and nano mechanics [17].

In this context, the AFM cantilever serves as the load of the beam and a deformation sensor (Figure 1.8). Measurements are performed along the axis of the beam obtaining force distance curves for each deformation (see Figure 1.9a), this allows to calculate the elastic constant of the beam for each instance, to then correlate the elastic constant with the distance of the measurement over the sample.

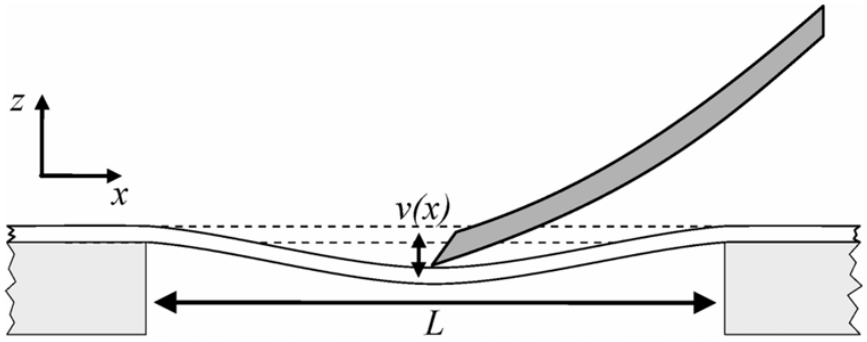

Figure 1.8: *Diagram of cantilever indentation over beam sample [23].*

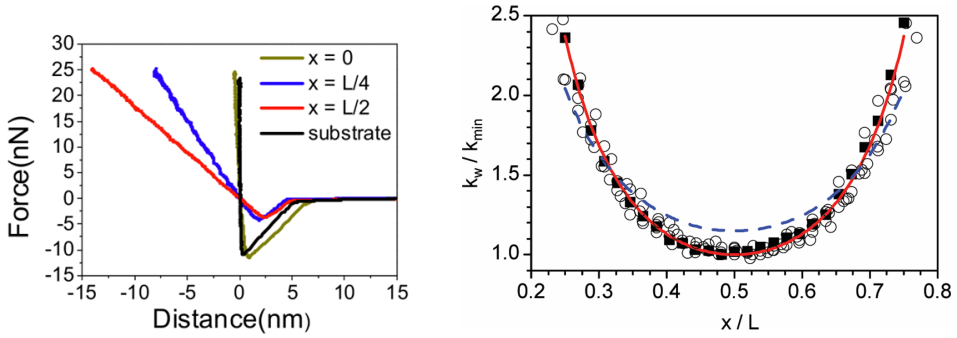

(a) (b)

Figure 1.9: (a)*Comparison of force distance curves for nano-mechanical bending tests along the beam length [12].* (b)*Plot of elastic constant values obtained from force curves along the beam vs. the position in the beam [23].*

Through this correlation, it is possible to obtain Young's modulus, considering certain characteristics of the beam, such as moment of inertia, and their boundary conditions to the substrate. From this two main models are widely used; simply supported beam model (SSBM) which assumes that the beam ends can freely rotate as a reaction of the applied load, and the double clamped beam model

(DCBM) which assumes that the ends of the beam are fixated to the support points. The equations that describe the elastic constant for each model are:

For DCBM:

$$k(x) = \frac{3L^3EI}{(L-x)^3x^3} \tag{1.25}$$

For SSBM:

$$k(x) = \frac{3LEI}{(L-x)^2x^2} \tag{1.26}$$

In both equations E is Young's modulus, I moment of inertia of the beam, L is the length of the beam and x the position in which the load is applied [23], [17], [10]. As the elastic constant is obtained through force curves along the length of the beam it is possible to plot them as a function of the position in the substrate and make a fit with the obtained equations, which will yield a value for Young's modulus [12], [23] as shown in Figure 1.9b.

Chapter 2

Experimental Setup and Procedures

During this investigation, there were various configurations in which the electrospun nanofibers were studied for mechanical testing, consequently this section will be divided into several parts addressing the production of the polymeric fibers for their different compositions and formats (single fibers and electro-spun mats), their deposition in various substrates and the corresponding measurement in AFM for topography and force spectroscopy. Furthermore, the techniques developed and used to measure the nanofibers in different conditions will also be explained, including the fabrication of colloidal probes, the configuration of humidity conditions in the AFM environmental chamber, and the post-analysis required to interpret the collected data.

2.1 Electrospun Nanofibers

In this section the protocols for producing the polymeric solution will be described. Most of these protocols were extracted from M. Taborda et al., [32]. The concentrations were replicated to maintain the electrospinability reported by M. Taborda et al.

2.1.1 PVA and PVA/SG/Ch blend

Firstly, for the solution of only PVA, polyvinyl alcohol should be dissolved in ultrapure water (Milli-Q) at a concentration of 10% w/v, at 70°C to 80°C for around one to three hours depending on the amount of solution that will be prepared. This polymer should be added to the already heated water at a slow rate (tip of plastic spatula) to avoid the formation of clusters and accumulations. When the solution is homogeneous, it should be left to cool down to room temperature.

Then, if it will not be used that day, it has to be stored in the fridge at around 3°C and covered.

Then for the blend of polyvinyl alcohol, salmon gelatin, and chitosan (PVA/SG/Ch), a solution of the three biomaterials should be mixed at 70 to 80 degrees Celsius and 350 stir on a heating plate. The proportions for the formulation are 50% of the final solution with PVA at 20% w/w concentration, 0.3 of the solution with salmon gelatin at 3% w/v concentration and 0.2 of the solution with chitosan at 3% w/v concentration, Obtaining a formulation of PVA (10% w/w), salmon gelatin (0.9%) and chitosan (0.6%).

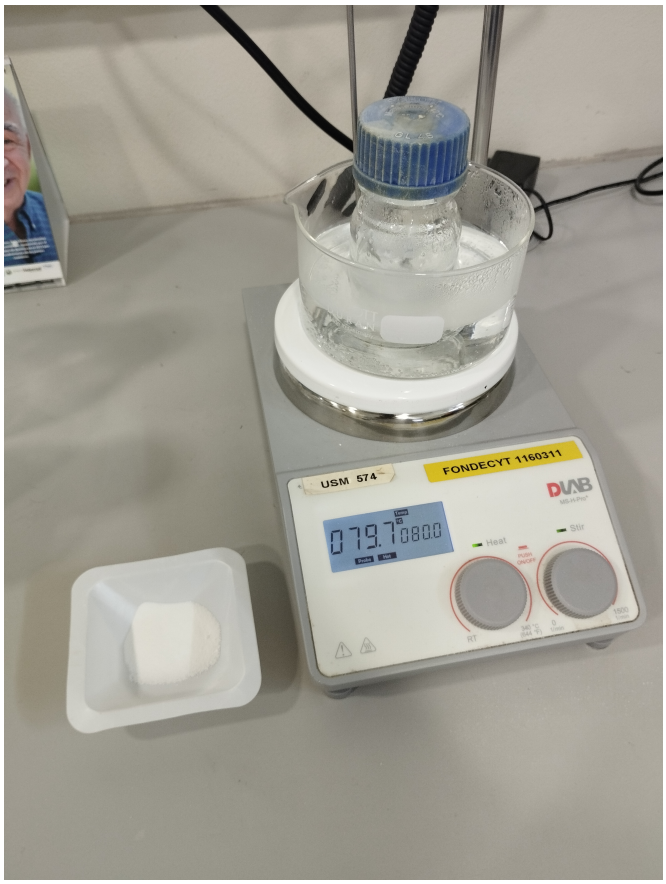

Figure 2.1: *Preparation of PVA solution in ultrapure water at 80 degrees Celsius, heater plate, PVA in white plastic pot.*

2.1.2 Electrospinning

For electrospinning, a homemade UTFSM electrospinning will be used together with a syringe pump (Figure 2.2). The following steps are taken if the solution is refrigerated:

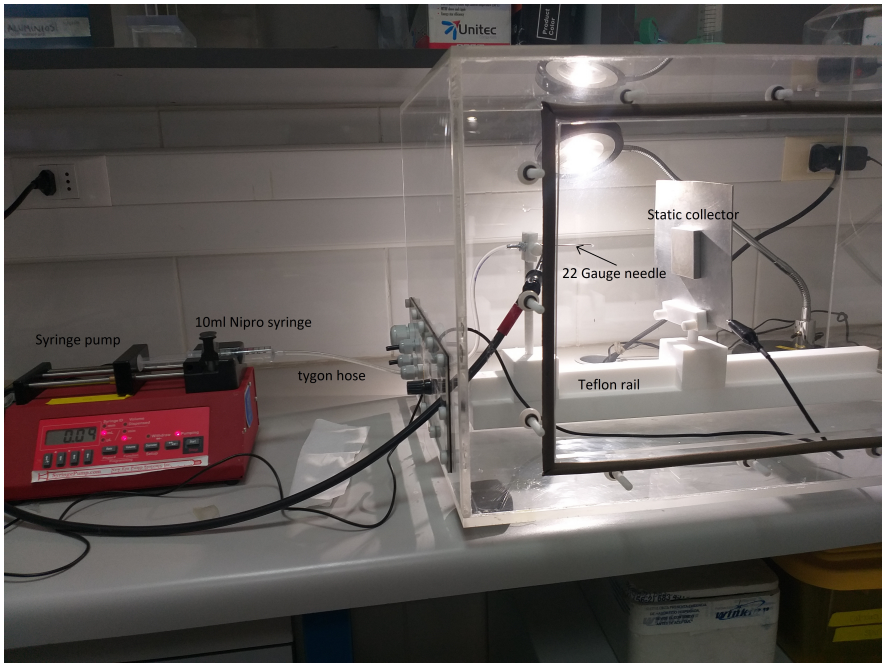

Figure 2.2: *Homemade electrospinning setup, with red syringe pump (New Era Pump Systems, Inc.) and 10mL Nipro syringe, connected through a Tygon hose into a 22 gauge needle supported by Teflon rail, finally pointing to a static collector.*

First we heat the stored solution in a thermoregulated bath at 70 °C. Once the temperature is reached heat the solution for 30 minutes with stirring at 250 stir and then 30 minutes at 500 stir, until a homogeneous solution is seen.

The electrospinning machine must be clean for the electrospinning to work properly. The cleaning protocol consists in the following points:

Clean the main chamber, clean the collector, 22 gauge (G) blunt needle (Ramé-hart instrument co, US) (Figure 2.3a), electrospinning hose (Ramé-hart instrument co, US) and dry them before use. Ensure that the 10mL Nipro syringes are not clogged, otherwise clean with ethanol 70%.

The pump system (New Era Pump Systems, Inc., USA), configured with the parameters to be used (0.8 mL/hr and the corresponding diameter of the syringe), should be connected. Finally, the voltage source (Figure 2.3b) must be connected and ready to be used at 9kV.

To electrospun the solution, it must be at room temperature, so it is recommended to let the mixture cool for about 30 minutes.

Then the electrospinning system is assembled. The 22 gauge (G) blunt needle is placed in the Teflon support and then the collector plate is locked in its respective support rail, making sure that it is 10cm away from the tip of the needle (distance needle-collector=10cm). The electrospinning hose is attached to the 22

(a) (b)

Figure 2.3: (a) *Cleaned 22 gauge blunt needle (Ramé-hart instrument co, US).* (b) *High voltage adjustable source for electrospinning.*

gauge (G) blunt needle, as shown in Figure 2.4. Then the positive (+) terminal of the voltage source is connected to the 22 (G) gauge blunt needle, and the electric ground of the power source is connected to the collector plate, closing the circuit.

If the solution has many bubbles, it is transfered to a 50mL Falcon tube and centrifuged at 1780rpm for 2min at 24^{o}C. Then using a 10mL Nipro syringe 10mL of the solution are taken to be electrospun. The syringe containing the solution to be electrospun is placed within the pump system (New Era Pump Systems). The other end of the electrospinning hose is connected to the syringe containing the polymer. Then without starting the voltage source, the pump is switched on and the flow rate is left to stabilize for about 10 minutes. Finally,the voltage source is switched on at 9 [kV] to begin electrospinning.

Single Nanofiber

To obtain single nanofibers over a surface, the following electrospinning protocol is used. When the Taylor cone is visible and stable, a substrate is positioned between the needle and the static collector for a few seconds (between 1 to 10 seconds depending on the deposition rate). To accomplish this, the substrate is adhered to an insulator using paper tape. This allows for a safer manipulation inside the electrospinning chamber. Finally, the nanofibers are checked on the substrate through an optical microscope to ensure that they are under optimal conditions, i.e, no beading nor spraying [43], [29].

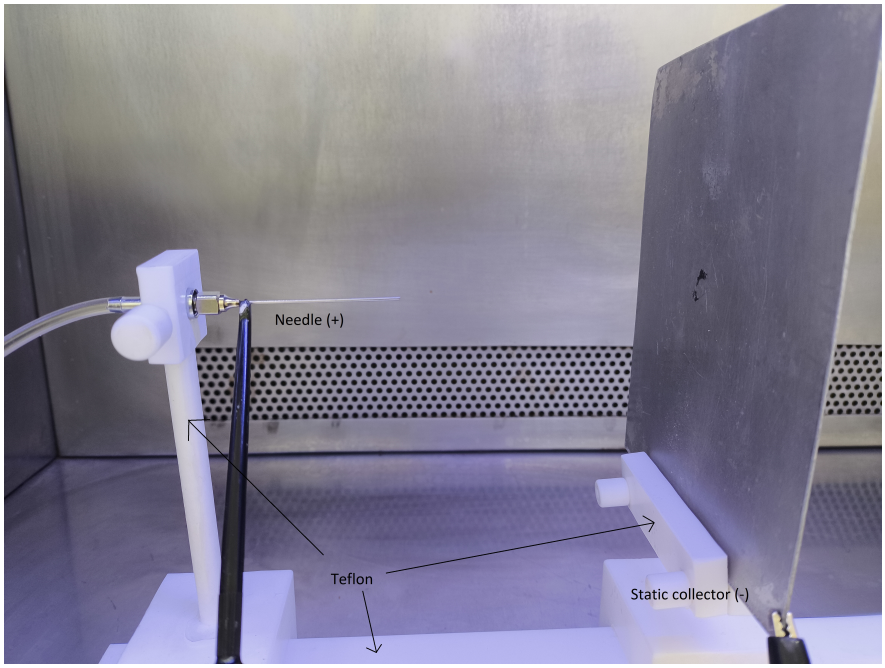

Figure 2.4: *Close up of the needle mounted in the Teflon structure, pointing to the static collector at a 10cm distance, positive connected to the needle and negative to the collector.*

Electrospun mat

In this case, the electrospinning is left to run for 4 hours using the static collector as a substrate to form a mat of nanofibers, which allows easier manipulation given the thickness of the scaffold. To remove the scaffold from the collector, tweezers are used starting from the corners of the synthesized mat. The thickness of the scaffold produced depends on the average diameter of nanofibers and the exposition time of the substrate under electrospinning, those produced in this research were in the ranges of 1 to 4μm.

2.1.3 Substrates for Nanofiber Deposition

During this investigation, several substrates were used for the testing of nanofibers, each providing different insights into the characteristics of the polymeric nanofibers and allowing for different measurement scales.

Silicon Wafer

The silicon wafers utilized for fiber deposition were of type P/B, 1 to 5 $m\Omega \cdot cm$ resist, a thickness of 280μm and single side polished (SSP). In this case, the silicon wafer was cleaned with ethanol and isopropanol before nanofiber deposition.

Electrospinning is performed for 5 seconds on the polished side, and then the density of fibers over the wafer surface is checked under an optical microscope; if there is not enough density, the deposition process is repeated.

AFM Calibration Grid

An AFM calibration grid from 'budget sensors' was utilized in the experiments, the die size of the grid is 5x5 mm and it presents rectangular and circular shapes, in the form of holes or protrusions made from silicon dioxide, the pitch of these shapes is 10 μm for the external region and 5 μm for the internal part, and its height (or depth in the corresponding case) is 500 nm (Figure 2.5)

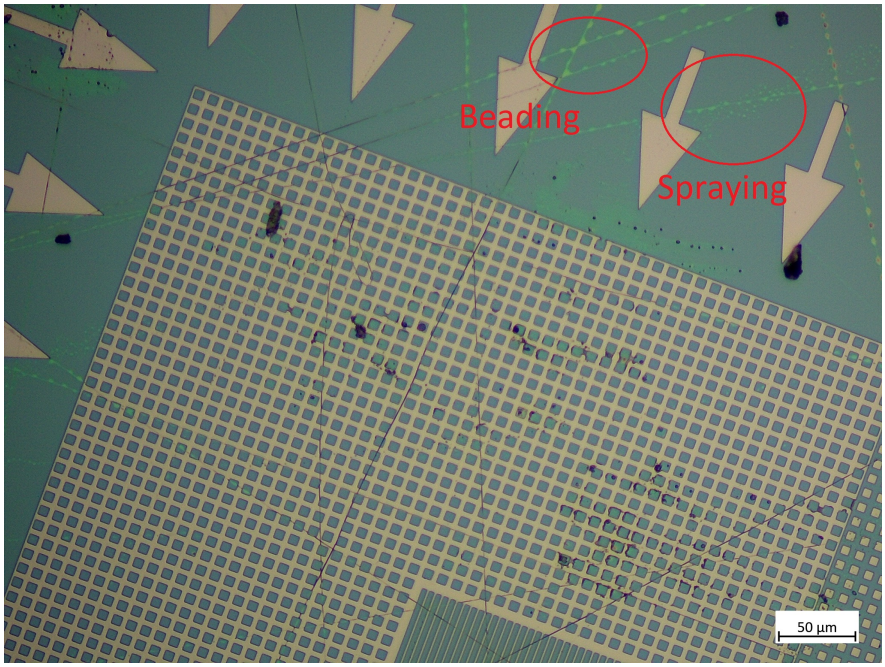

Figure 2.5: *AFM calibration grid observed under microscope with nanofibers already deposited over it. Beading and spraying can be appreciated in the up right corner.*

Micro-structured Grid Prepared by Photolithography

To obtain a better deformation range for the fibers, a microstructured grid was created with a depth greater than the calibration grids. It was produced by lithography using SU8 as a mask and etching the silicon wafer to obtain deeper patterns of 5 μm depth, also with greater separation between the peaks reaching 40 μm. (Figure 2.6a)

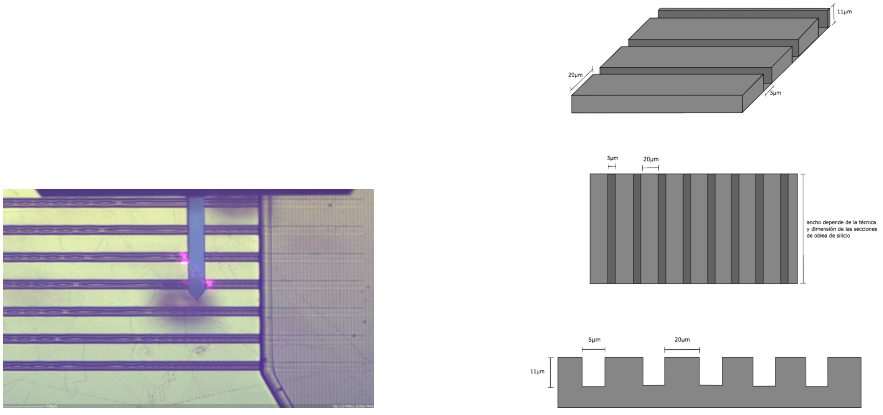

(a) (b)

Figure 2.6: (a)*Etched microstructure produced on silicon grid by photolithography for polymeric nanofiber mechanical testing, well width of 40µm and depth of 5µm.* (b)*Preliminary digital design for the etched microstructure for nanofiber mechanical testing, measures where changed during the production due to equipment limitations.*

2.2 Colloidal Probes

To measure the mechanical modulus of the nanofiber mat, colloidal probes were used with the objective of comparing these values to those obtained on single nanofibers. The colloidal probes were manufactured from a tipless cantilever (TL-FM from nanosensors) and silicon beads of 10 μm. Firstly, the beads are dissolved in ultrapure water (milli-Q) to have less bead density; then a drop ($10^{-9}\mu l$) is deposited on a glass slide with a micro pipette. In second place, the tipless cantilever is adhered on a 3-axis hydraulic micromanipulator (Narishiga, Japan) and monitored under an optical microscope. The cantilever is aligned and barely out of focus, so the glass slide and beads are clearly seen. Then a two-component epoxy glue is prepared and deposited on the other side of the glass slide, the tipless cantilever is approached onto the glue from upside down and barely touching its surface (Figure 2.7a), the excess is removed by pressing the cantilever over the clean surface of the glass slide several times; in this work, this was done between five and seven times to ensure a very small droplet of epoxy glue. Finally, the cantilever is approached from the top to the bottom to a bead isolated from the rest, as it will make it easier to attach only one to the cantilever, as shown in the figure (Figure 2.7b).

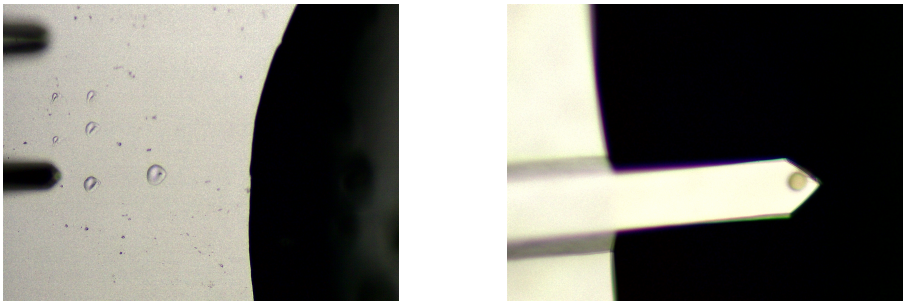

(a) (b)

Figure 2.7: (a) *Microscopic image of two component epoxy glue, acquiring a droplet with a tipless cantilever.* (b) *Tipless cantilever (TL-FM) with a silicon sphere attached to the tip using a two component epoxy glue.*

2.3 Environmental Chamber

To vary the humidity and monitor the mechanical and morphological changes in the fiber, it was necessary to implement an environmental chamber on the Flex AFM system (Nanosurf, Switzerland), this will isolate the variables such as temperature, pressure and humidity. The chamber is fairly easy to mount, it has to be screwed into the substrate holder of the AFM making use of viton rings to seal it. Then, as the head of the equipment is placed (Figure 2.8a), a magnetic surface will join the head of the microscope to the environmental chamber sealing it with another viton ring.

2.3.1 Humidity Sensor

To monitor temperature, pressure and relative humidity, a BME-280 sensor (Figure 2.8b) was installed that can measure relative humidity, pressure and temperature in real time, this sensor goes into the chamber and is connected to a controller and monitoring system developed using LabVIEW.

2.3.2 Humidity Control

In this work the main form of relative humidity (RH) control was through saturated salt solution that stabilize at certain humidities. In this case, these salts were lithium chloride ($LiCl$) for low RH values and potassium nitrate (KNO_3) for higher RH values [35]. The lithium chloride solution should be at least 68 grs per 100 grs of H_2O, but in practice, it was easier and faster to oversaturate the solution by adding a small amount of water to the salt. For potassium nitrate, the proportions were 40 grs of KNO_3 per 100 grs of H_2O. Both of these solutions were contained in a small Petri dish, so it could fit inside the AFM chamber

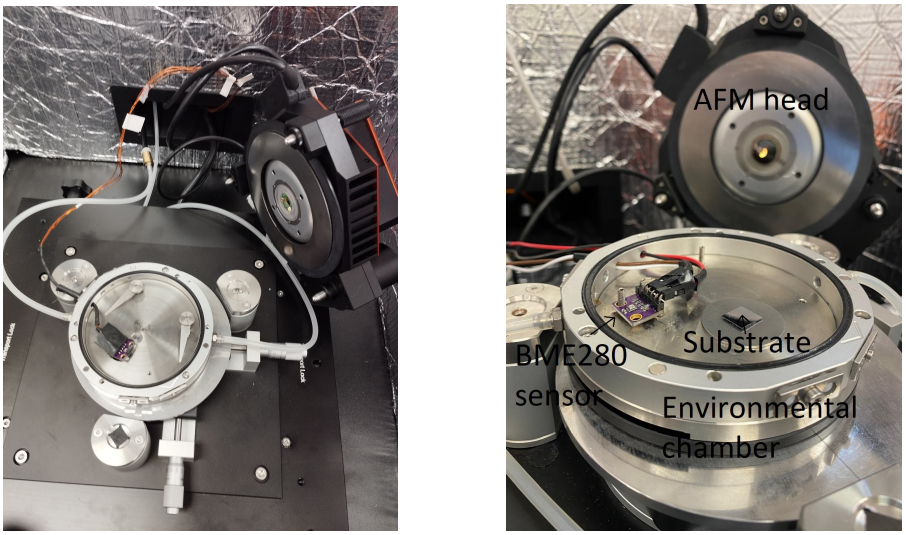

(a) (b)

Figure 2.8: (a)*Nanosurf AFM with screwed on environmental chamber and humidity sensor attached.* (b)*BME-280 sensor for relative humidity, pressure and temperature, installed inside the AFM environmental chamber.*

along the substrate. After the corresponding solution is ready, it will be left in the chamber until the RH stabilizes.

2.4 AFM Measurements

Over the course of this research, the main tool to measure the mechanical properties and morphology of the fibers will be AFM, mainly using force spectroscopy and tapping mode, respectively. The preparation of the environmental chamber and the substrate has to be done before anything related to the AFM. Firstly, the cantilever is mounted on the holder, then the holder is adhered to the AFM head, which contains magnets to secure the holder. Secondly, the laser is aligned with the screws on top of the AFM head, seeking that the laser spot that appears in the camera is in the tip of the cantilever, the intensity registered by the photodiode is above 20% and correctly centered. Then we select the AFM tip that is going to be used (TL-FM or PPP-FMR in this case, depending on the measurement). The remaining steps depend on the protocol that is going to be followed (Topography or Force Spectroscopy).

2.4.1 Topography

Continuing from the last section, to perform "tapping-mode" the phase contrast option is selected, the first step is to obtain a frequency sweep yielding the elastic

constant of the cantilever and its resonance frequency. For this, the software has an inbuilt function to obtain the resonance frequency of the cantilever. Then the tip is approached to the substrate via manual screwing, and for fine approaching, the system has a stepper motor to approach with better precision, and to finally engage the tip the "approach" button on the software is pressed, completing the approaching process. Finally, setup values are arranged, the "setpoint" is set to a high percentage to minimally interact with the sample, typically 70% was used during this investigation.

2.4.2 Force Spectroscopy

Starting from the general setup, for this type of measurement, it is required that we do some additional calibration, the mode is set to static force and a thermal tuning routine is performed to obtain the elastic constant of the cantilever, after a few seconds of recording thermal noise the automatic fitting is performed and the elastic constant is determined. Then it is necessary to obtain the sensitivity of the cantilever to relate the distance of deflection to the potential difference measured (V) by the photodiode. This process consists of a force distance curve performed on a stiffer surface than the cantilever (typically silicon wafer or glass slides) [20]. When both calibrations are done the approaching process begins, in the same way as the previous step. Finally, the deflection is set as stop by value, considering a maximum force applied to the fiber in study.

Force Map

In general when fibers are tested mechanically through AFM, a force map is carried out, which consists of performing force curves over a grid with a specified distance between every deflection. The result is similar to a topography image in the sense that this force map is color coded with the brightness of pixels for higher values. The force map yields 3 channels stiffness, adhesion and Young's modulus.

Three-Point Bending

The main difference between this method and the previous one is that higher precision is required, so instead of a map, the deflection curves are performed on a straight line. For this, the fiber must be as stable as possible, this means that the sample must be fixed to the substrate, the chamber should be sealed, and temperature variations should be kept to a minimum, this is achieved by letting the AFM stabilize in a constant environment for several minutes. In addition, a previous topography image is highly recommended to have a notion of where the fiber is, so in the spectroscopy tab this image can be imported to draw a straight line over the fiber as shown in Figure 2.9.

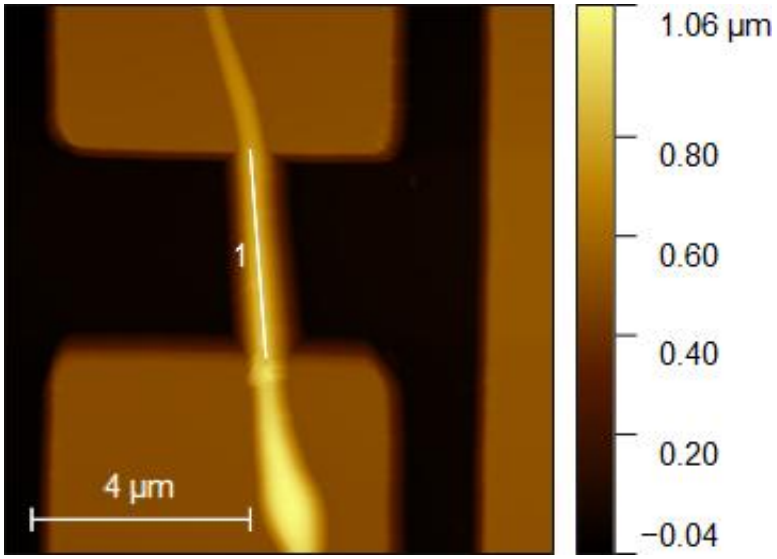

Figure 2.9: *Representation of straight line (1) where force curves will be performed over reference image.*

2.5 Data analysis

To obtain the data from the force curves in general and analyze through the Hertz model approximation, the software utilized was ANA (from Nanosurf).

Then to analyze three-point bending data, a simple Python software was developed; this software will take the force curves extracted from ANA in a CSV file, convert them into data frames, identify the linear section of the force curve (elastic deformation) and fit a linear function to it, obtaining its slopes. These slopes were plotted in an elastic constant vs. distance graph, in conjunction with a fitting function for the cases of a simply supported beam (SSBM) and a double clamped beam (DCBM).

Chapter 3

Results and Analysis

In this chapter, results obtained from the different methods in which nanofibers were studied are presented, separating them into three main sections. Nanofiber mats characterized by a colloidal probe, single nanofiber mechanics supported over silicon substrates, and three-point bending tests on suspended nanofibers. For all cases, studying their mechanical properties through AFM force spectroscopy complimenting them with topographical imaging, in order to obtain Young's modulus (E) as a function of relative humidity (RH). These measurements were performed on two types of polymeric nanofibers, Polyvinyl Alcohol (PVA 10%) and a blend of PVA, Salmon Gelatin and Chitosan (PVA/SG/Ch). Aiming to yield on the main mechanical differences of these polymers under humid conditions for scaffold performance.

3.1 Electrospun mat

Through colloidal probe testing, the mechanical properties of electrospun mats were obtained, assuming the colloid as a perfect sphere of radius $10\mu m$ and the substrate as an infinite plane. In the case of dry PVA/SG/Ch mats, force distance curves presented little to no *snap in* in comparison with the adhesion force, a slight non linear deformation at the end of the deflection and a clear adhesion to the substrate as shown in figure 3.2a.

Through the Hertz model, knowing the radius of the colloid, its Poisson's ratio, and repeating this process a statistically robust amount it is possible to obtain an estimated Young's modulus for the nanofiber mat.

The mean value for PVA/SG/Ch mats in dry conditions ($10\%RH$) is $47 \pm 19.89kPa$, the histogram took into account 153 force curves performed on the nanofiber mat, with a force of (check). The accuracy of the data is not ideal (Figure 3.2b), since the deviation was comparable to the mean value. Although this is a problem, the obtained value for Young's modulus can still be compared to that of the liquid environment (PBS medium).

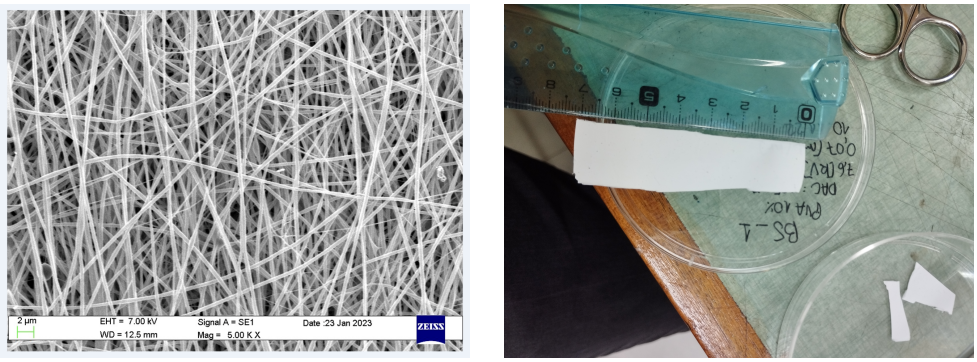

(a) (b)

Figure 3.1: (a)*Force distance curve for PVA/SG/Ch blend fiber mat in dry conditions, measured with colloidal probe, approach (blue) and withdraw (red) motions.* (b)*Histogram of Young's modulus obtained by indentation of colloidal probe over PVA/SG/Ch electrospun mat in dry conditions with mean* $47.10 \pm 19.89 kPa$.

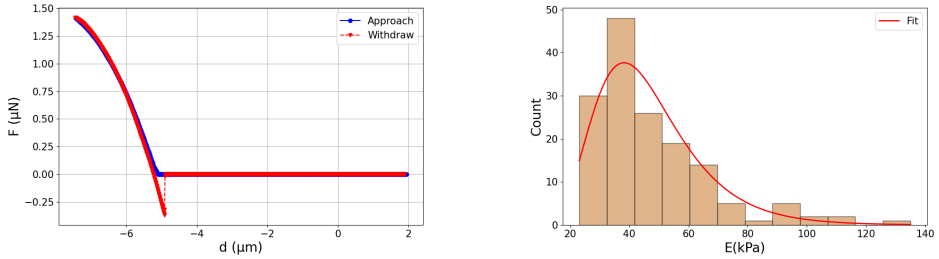

(a) (b)

Figure 3.2: (a)*Force distance curve for PVA/SG/Ch blend fiber mat in dry conditions, measured with colloidal probe, approach (blue) and withdraw (red) motions.* (b)*Histogram of Young's modulus obtained by indentation of colloidal probe over PVA/SG/Ch electrospun mat in dry conditions with mean* $47.10 \pm 19.89 kPa$.

The case of a PBS submerged mat showed a variation in mechanical modulus compared to the dry state. This can first be recognized by the behavior of the force curves (figure 3.3a), a clear hysteresis can be observed, which suggests either an attractive interaction with the surface during the withdraw or a "trapping" effect of the fibers since the probe will be pushed through them during the approach. Attractive forces during the approach motion are barely noticeable due to the adhesion being so high, and the scale of the colloidal probe and the fiber mat.

The histogram of figure 3.3b then shows a certain decrease in Young's modulus by at least an order of magnitude, obtaining a mean of 1.82 kPa and a deviation of 1.19 kPa, which allows for a grate comparison of both systems; the case of dry

environment shows a higher mechanical modulus than the mat in PBS medium. On the other side, the accuracy problem remains, meaning that something in the process is affecting to the measurements to come clean, e.g. the nanofiber mat is not homogeneously adhered to the silicon surface, or simply the nature of the problem being a mostly random system produces higher variance in the gathered data.

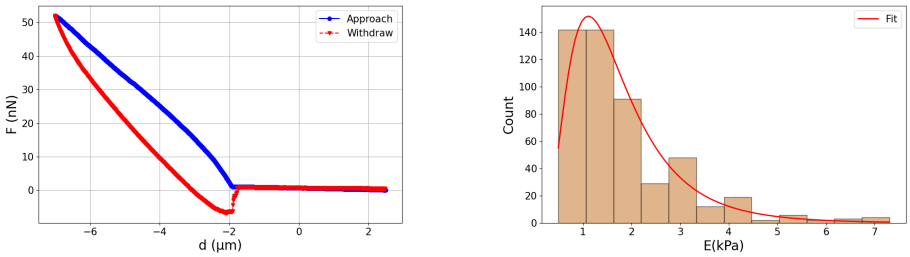

(a) (b)

Figure 3.3: (a)*Force distance curve for PVA/SG/Ch blend fiber mat submerged in PBS, measured with colloidal probe, approach (blue) and withdraw (red) motions.* (b)*Histogram of Young's modulus obtained by indentation of colloidal probe over PVA/SG/Ch electrospun mat submerged in PBS with mean* $1.82 \pm 1.19 kPa$.

In this case, it seems to be mostly due to the approximations that are being done to fit the Hertz model, since it assumes homogeneous and isotropic bodies and the nanofiber mat is neither isotropic nor homogeneous, which does not allow for the interpretation of one point of contact between both surfaces.

In future works to correct this issue there are a couple of actions that can be taken, first the size of the colloidal probe should be higher to account for the irregularity of the nanofiber mat surface, and better approximate to the infinite plane versus deflecting sphere. On the other hand, Hertz model may have too many conditions that are not meeting for the model to correctly predict the phenomena, a good alternative may be using the Johnson-Kendall-Roberts theory (JKR) [15], which adds a layer of viscosity and damping to the system, making it a better fit than the Hertz model.

3.2 Single nanofiber mechanics

To characterize the mechanics of a single nanofiber, AFM force spectroscopy was performed, using a normal AFM tip of radius $8nm$, in the first instance over a single PVA nanofiber deposited on a silicon wafer (as shown in Fgure 3.4) under different conditions for relative humidity (RH). In the dry state of 10% RH the force curve (figure 3.5a) exhibits a snap in in the approach motion, little or no hysteresis, meaning no significant plastic deformation is produced and a higher adhesion force in the withdrawal.

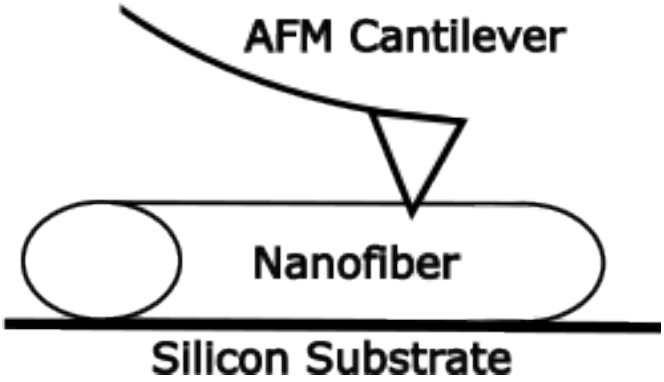

Figure 3.4: *Representation of the setup for the single nanofiber experiment over a silicon surface*

As presented in Figure 3.5b, the mean value for Young's modulus is $53.19 \pm 17.92MPa$, which accounts for a stiffer system than the electrospun mat, in multiple orders of magnitude. This could be due to the robustness of polymeric nanofibers in contrast to the complete mat, where fibers may slip from each other, detach from the substrate, or absorb more water due to the high porosity of the material.

In the humid case with 60% RH (figure 3.6a), the withdrawal shows clear hysteresis, meaning that there is deformation involved and even multiple contact points in the detachment.

The mechanical modulus ($3.86 \pm 3.23MPa$) decreases by one order of magnitude, very similar to the behavior seen in the PBS submerged mat case for the colloidal probe experiment.The error in this humid case is too high to be ignored, where the standard deviation is close to the actual value. This issue is most likely caused by the substrate in which the measurements are performed. Because nanofibers are softer than the substrate, the method can be sensing the stiffness of the silicon wafer. In addition, the indentation of the AFM tip could be

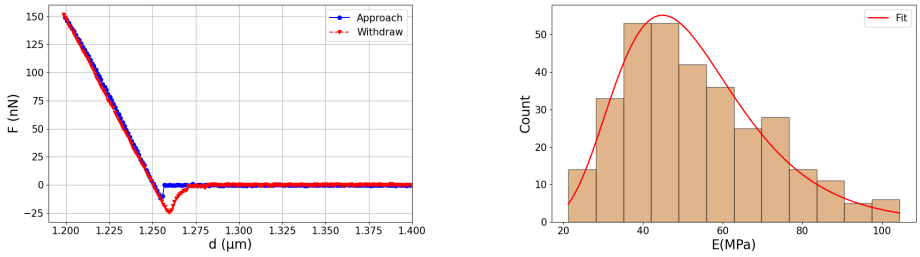

(a) (b)

Figure 3.5: (a)*Force distance curve for PVA single nanofiber in dry environment (*10% *RH), measured with standard AFM tip, approach (blue) and withdraw (red) motions.* (b)*Histogram of Young's modulus obtained by indentation of AFM tip in dry environment (*10% *RH) with mean* $53.19 \pm 17.92 MPa$.

perforating the nanofiber since it is being pressured from both the end of the tip and the hard silicon substrate, which could explain the hysteresis in Figure 3.6a. So, to account for both problems, the method of measurement and the model to encounter Young's modulus will be changed.

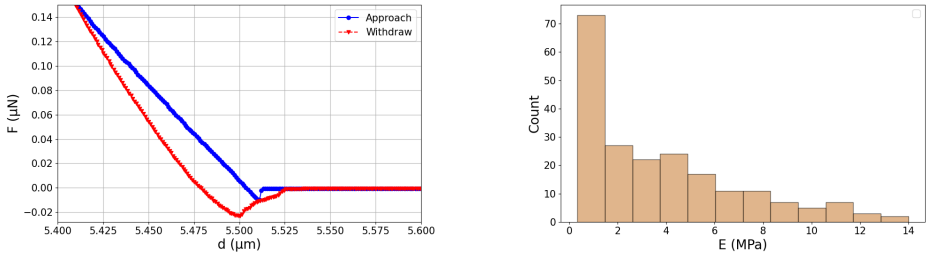

(a) (b)

Figure 3.6: (a)*Force distance curve for PVA single nanofiber in humid condition (*60% *RH), measured with standard AFM tip, approach (blue) and withdraw (red) motions.* (b)*Histogram of Young's modulus obtained by indentation of AFM tip in humid conditions (*60% *RH) without fitting curve due to the dispersion of the data and the inaccuracy it may provide, with mean* $3.86 \pm 3.23 MPa$.

The proposed solution to these measurement problems will be to perform the mechanical characterization of the nanofibers through three-point bending experiments, this way the measurements will not depend on the shape and radius of the AFM tip, as the spectroscopy will be performed over the center of the fiber the slipping will be reduced and the stiffness of the substrate will not intervene with the measurements of the soft nanofibers. All of this could reduce the previous observed dispersion of the gathered data.

3.3 Three-Point bending of suspended nanofibers

Firstly, the force curves are obtained in a similar way to the previous cases, with the exception that they are performed on a straight line over the suspended nanofiber; to accomplish this accurately, a topography scan is performed. If the image shows that the nanofiber is suspended, it can be seen through longitudinal cuts and a comparison with the substrate, as shown in Figure 3.7 for a PVA nanofiber under dry conditions of 24% RH.

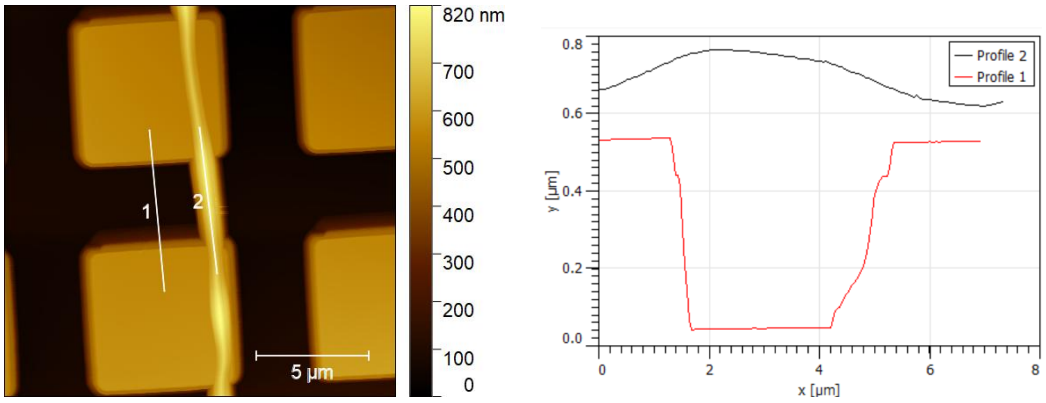

(a) (b)

Figure 3.7: (a) *Topography image of the nanofiber suspended over AFM calibration grid.* (b) *Line profile comparison between the suspended nanofiber and the silicon structure.*

As force measurements are performed along the nanofiber, multiple force curves are obtained, each with a different elastic constant, because the stiffness sensed by the cantilever decreases as the deformations are closer to the center of the fiber. This can be observed in the slope of the force curves shown in Figure 3.8.

In addition, not only does the slope vary, but the adhesion force in the withdrawal increases as the measurement is performed close to the center, most likely due to the lack of substrate interacting with most of the nanofiber.

Then the slope obtained for every indentation is plotted in a distance vs. elastic constant (k) graph (Figure 3.9), which can be fitted by beam deformation models. Since the interaction of the fiber with the silicon structure supporting is not clear, it is difficult to assess which model, DCBM or SSBM, will better model this system. Because of this, both cases will be taken into account, comparing them in the process of establishing the more accurate model.

As shown in Figure 3.9, the fit with less error and better R^2 will correspond to the simply supported beam model (SSBM). The mechanical modulus obtained for the PVA nanofiber under dry conditions is $E = 7.96$ with little to no fitting error.

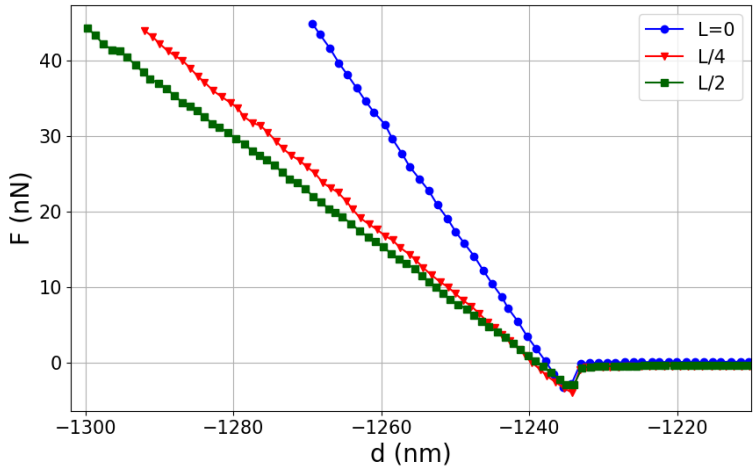

Figure 3.8: *Force curves of suspended nanofiber along its elongated axis, the change in their slopes account for a change in elastic constant due to proximity to support point. Blue, indentation at start point $L = 0$. Red, indentation at $L/4$. Green, indentation at $L/2$.*

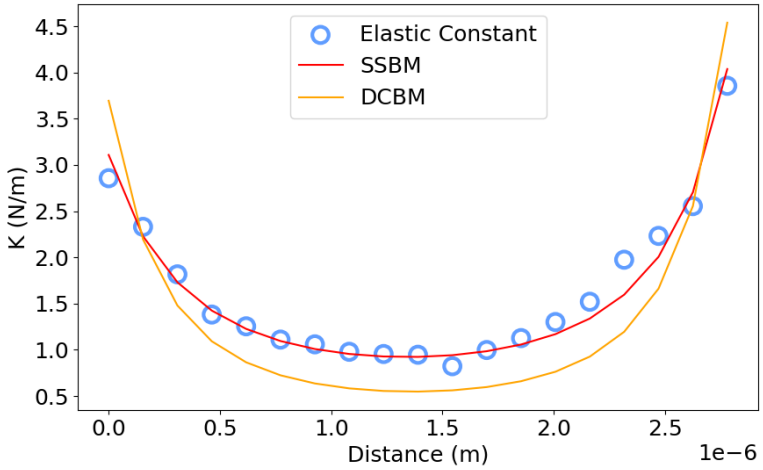

Figure 3.9: *Elastic constant vs distance along the PVA nanofiber at 24% RH graph, with both models fitting the data. SSBM: $E = 7.96 \pm 1.52 \times 10^{-34} GPa$ ($R^2 = 0.97$), DCBM: $E = 1.18 \pm 1.09 \times 10^{-33} GPa$ ($R^2 = 0.63$)*

For future data both fits will still be tested, to accurately find the mechanical modulus.

The modulus for the case of 50% RH shows the same tendency to fit better with the SSBM model, and a slight decrease in the young modulus is observed

as the relative humidity increased. The R^2 value is not that optimal due to some inaccuracy but is still a better approach than the previous methods to obtain Young's modulus.

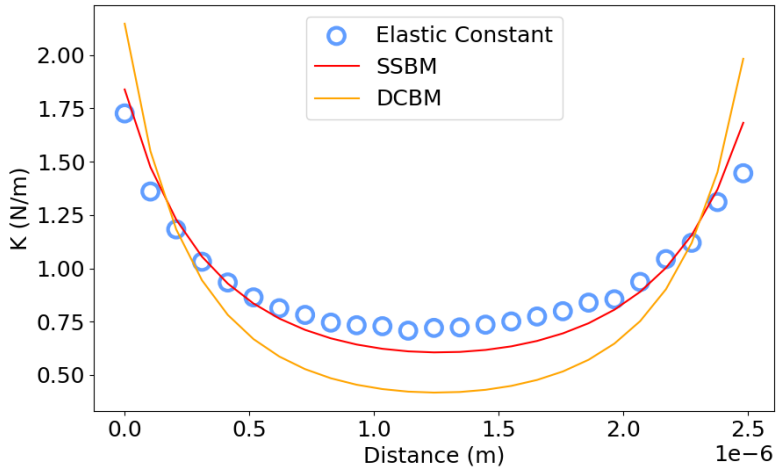

Figure 3.10: *Elastic constant vs distance along the PVA nanofiber at* 50% *RH graph, with both models fitting the data. SSBM:* $E = 6.79 \pm 0.138GPa$ *(*$R^2 = 0.88$*), DCBM:* $E = 1.17 \pm 0.068GPa$ *(*$R^2 = 0.02$*)*

For the PVA nanofiber, the last case is at 72% RH, decreasing the mechanical modulus by an order of magnitude compared to the previous case. As can be observed in Figure 3.11, the data points appear flattened at $0.15N/m$, this can be produced by the cantilever tip sliding off the nanofiber, making it appear to have different mechanical properties as the fiber deforms, or by a change in the behavior on the surface of the material, as humidity increases, an increasing layer of water molecules is formed on the surface of the nanofiber, changing the attraction and repulsion forces during the contact regime.

Then, the cases with the blended polymer (PVA/SG/Ch) were studied for three different humidity values, in ranges similar to those in the previous case. In the first instance, at 27% RH the mechanical modulus of $E = 26GPa$ is higher than that obtained for PVA nanofibers under similar conditions, hinting at a rise in their stiffness, as expected from previous studies. Once again, it is shown in Figure 3.12 that the best fitting corresponds to the SSBM.

As relative humidity increases in the environmental chamber, the mechanical properties are expected to drop, and for blended nanofibers at 50% RH this decrease is drastic, as Young's modulus decreases to $E = 1.32GPa$, a drop of about one order of magnitude. This may indicate that the composition of PVA/SG/Ch is responding more to variation of humidity in the environment. This may be

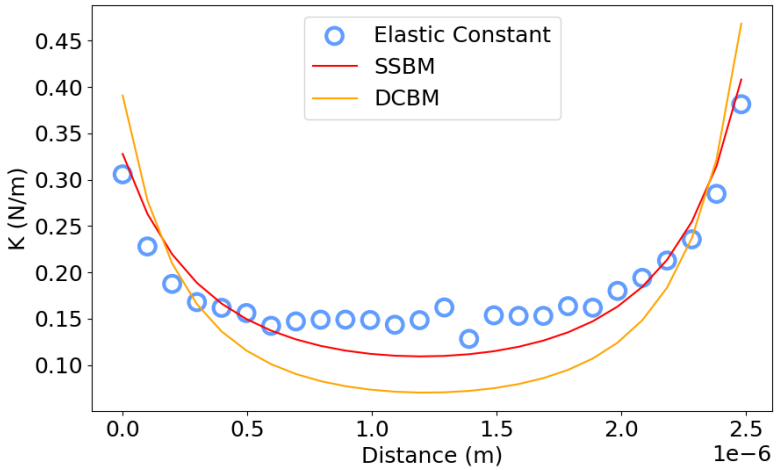

Figure 3.11: *Elastic constant vs distance along the PVA nanofiber at* 72% *RH graph, with both models fitting the data. SSBM:* $E = 0.552 \pm 0.0164 GPa$ $(R^2 = 0.78)$*, DCBM:* $E = 88.7 \pm 6.03 MPa$ $(R^2 = 0.07)$

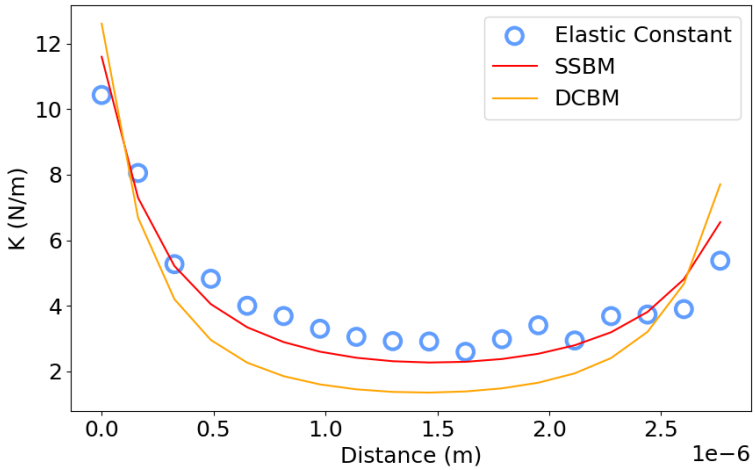

Figure 3.12: *Elastic constant vs distance along the PVA/SG/Ch nanofiber at* 27% *RH graph, with both models fitting the data. SSBM:* $E = 25.9 \pm 1.38 \times 10^{-34} GPa$ $R^2 = 0.870$*, DCBM:* $E = 3.85 \pm 7.85 \times 10^{-34} GPa$ $R^2 = 0.368$

due to the high crystallinity in pure poly vinyl alcohol nanofibers in contrast to the blended ones. The graph in Figure 3.13 shows a good fit through the simply supported beam model.

The last case for PVA/SG/Ch nanofibers is at 70% RH, as the trend follows, the SSBM fits better for the data obtained in this case. However, Young's modu-

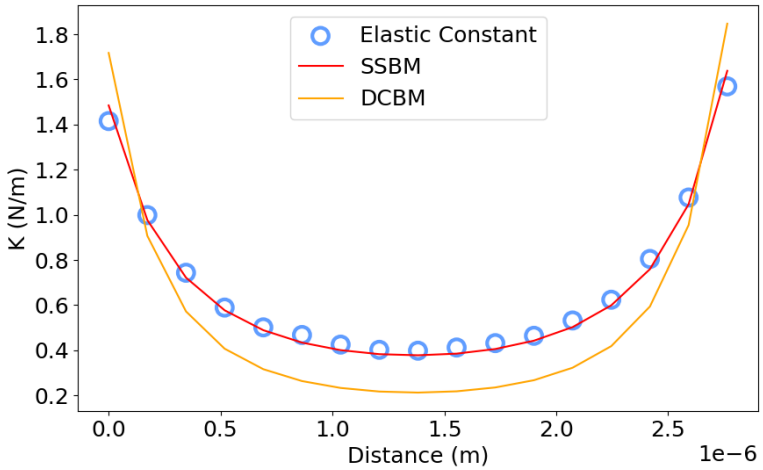

Figure 3.13: *Elastic constant vs distance along the PVA/SG/Ch nanofiber at* 50% *RH graph, with both models fitting the data. SSBM:* $E = 1.32 \pm 2.10 \times 10^{-34} GPa$ $R^2 = 0.991$, *DCBM:* $E = 0.186 \pm 2.89 \times 10^{-33} GPa$ $R^2 = 0.678$

lus seems to stagnate at $E = 1.24 GPa$. The variance in this case with respect to the previous one is much smaller than the decrease in stiffness between the cases of 27% and 50% RH.

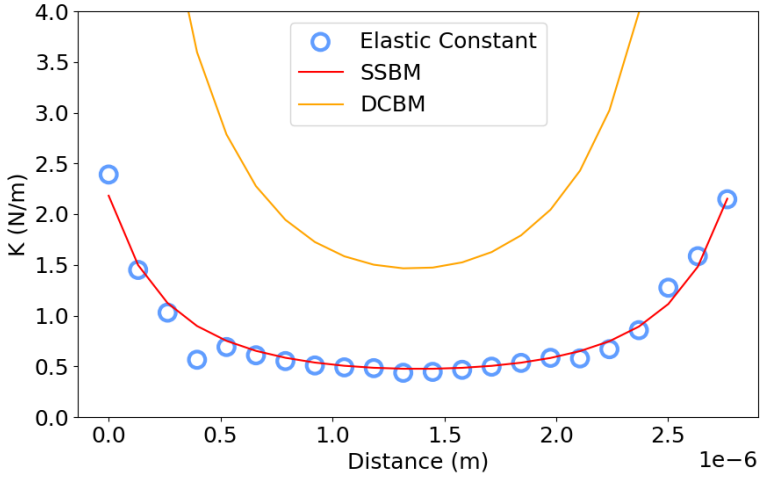

Figure 3.14: *Elastic constant vs distance along the PVA/SG/Ch nanofiber at* 70% *RH graph, with both models fitting the data. SSBM:* $E = 1.24 \pm 5.40 \times 10^{-35} GPa$ $R^2 = 0.966$, *DCBM:* $E = 0.952 \pm 2.78 \times 10^{-33} GPa$ $R^2 = -69.8$

To summarize these results, it is useful to plot the mechanical modulus ob-

tained for each instance of relative humidity, and then compare between PVA and blended nanofibers.

In Figure 3.15, it is easy to appreciate the difference in the mechanical modulus between PVA and blended nanofibers, the latter presents a higher modulus for drier states, while PVA fibers vary less in their modulus as humidity increases. This is likely due to their composition, since a blend of biomaterials (PVA, salmon gelatin, and chitosan) is less likely to polymerize in crystalline structures. Its response to humid environments is enhanced, as they probably present multiple defects in their structure and interfaces between the materials, allowing for greater space for water molecules to allocate and a lower energy barrier for them to infiltrate in the material (since the blend is not ordered). Furthermore, the addition of chitosan to the solution is likely adding to the mechanical stiffness of the blend as shown by Ullah et al. [36], the addition of chitosan in conjunction with fish collagen tends to increase the tensile modulus of the resulting material, explaining why Young's modulus is higher in the blended case than in the PVA nanofibers.

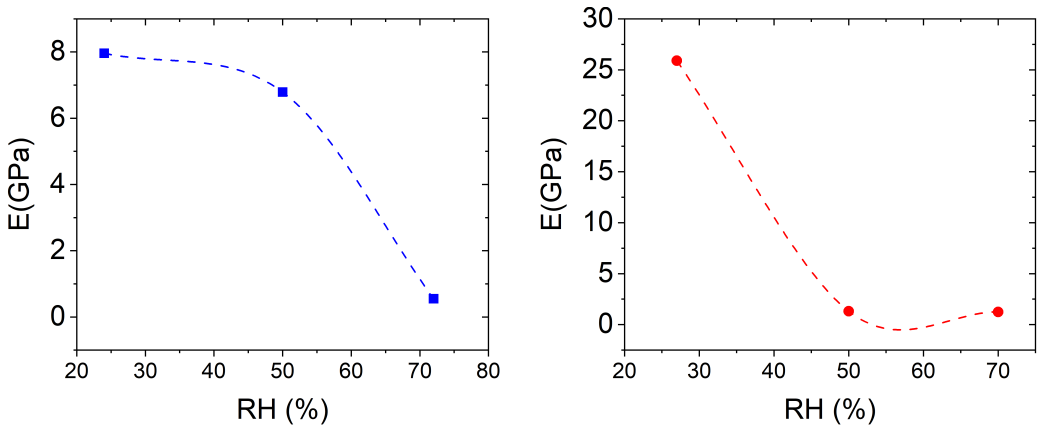

(a) (b)

Figure 3.15: *(a)Young's modulus $E(GPa)$ for PVA nanofibers obtained through three-point bending test at different relative humidities $RH(\%)$. (b)Young's modulus $E(GPa)$ for PVA/SG/Ch nanofibers obtained through three-point bending test at different relative humidities $RH(\%)$.*

In both cases (Figure 3.15), it is observed that the mechanical modulus drops in a considerable amount after a certain threshold with the increase in relative humidity, which yields a change in the behavior of the material from a semi-crystalline polymer to a rubbery state, as shown mainly by the sudden decrease in Young's modulus and the greater plastic deformation under humid conditions (see Figures 3.6a, 3.3a). Hence, these polymeric nanofibers exhibit a glass transition induced by relative humidity in their environment at constant temperature

[19]. This threshold depends on the composition of the nanofiber, as shown in Figure 3.15 the glass transition induced by humidity is lower in the PVA/SG/Ch nanofibers.

3.3.1 Micro-structured Grid for nanofiber mechanical testing

To corroborate that the nanofibers are in a glassy state before the relative humidity threshold, it is proposed to perform fracture tests on them by means of indentation. The problem that arises is that the AFM calibration grid does not have the minimum depth to elongate the nanofiber enough to reach its breaking point. Therefore, it is necessary to use a grid made by photolithography with larger depth dimensions.

The photolithography grid was applied for measurement of three-point bending experiments, as described in the previous case with the AFM calibration grid, yielding some preliminary results shown in Figure 3.16.

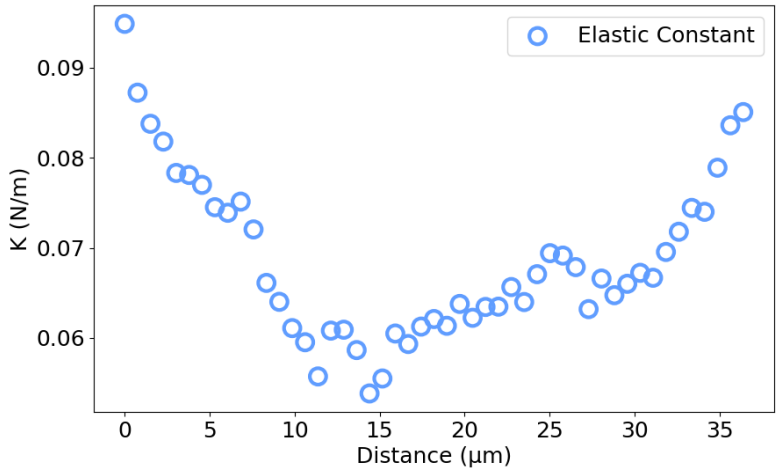

Figure 3.16: *Elastic constant vs distance along the PVA nanofiber at* 30% *RH graph, without the models fitting the data. In both cases the models did not adjust successfully, yielding high variance between the fit and the data.*

These results can not be interpreted directly like previous ones, this might be because the conditions for the micro-structured grid are vastly different than the AFM calibration grid, i.e, the dimensions of the system are vastly larger, producing more variance along the fiber and the border conditions are more complex than the nanoscopic case.

If the force curves in the previous measurement are observed (see Figure 3.17), the snap-in is not visible during the approach denoting a repulsive interaction in-

stead of the usual attractive force, but as the withdraw is performed the nanofiber behaves as usual presenting the adhesion force near the supposed zero distance point. As these results are preliminary there is not enough data to draw to conclusions about this behavior, other than having to repeat these experiments. Also, it is necessary to perform breaking point experiments in these nanofibers suspended over the new micro-structured grid to determine if the material is presenting the mechanical properties of a glassy semi-crystalline polymer, under the variance of relative humidity.

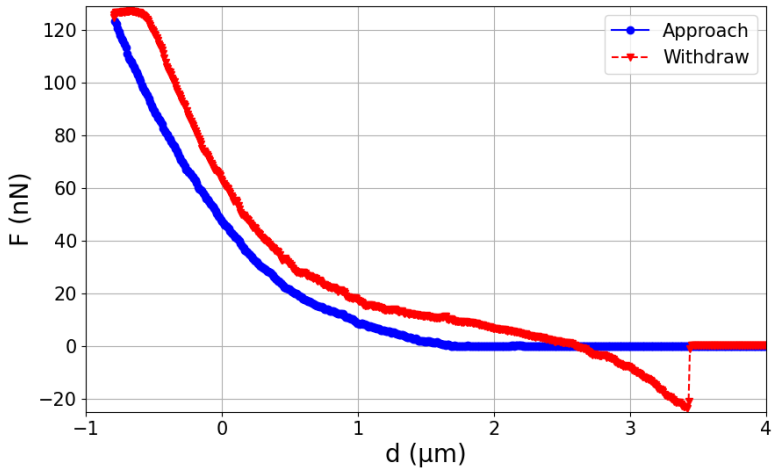

Figure 3.17: *Force (nN) vs distance (µm) curve of a suspended PVA nanofiber under slightly dry conditions (30%RH).*

Chapter 4

Conclusions and Future work

This research inquired in the process of fabrication and characterization of polymeric nanofibers mixed with biopolymers to adjust their mechanical properties and interaction with cells. Through electrospinning, it was possible to produce large amounts of nanofibers to study their properties under different environmental conditions such as relative humidity. In addition it was possible to take a glance at some scalable properties of nanofiber based scaffolds in their mechanical characterization, such as stiffness of electrospun mats in comparison with isolated nanofibers.

For this several techniques and methods were implemented, firstly, colloidal probe testing allowed for the measurement of Young's moduli for electrospun scaffolds in environmental and liquid conditions. Relative humidity control on an environmental AFM chamber, with pressure, temperature, and humidity sensors to manage the conditions of the nano mechanical experiments. Low-exposure electrospinning, to obtain isolated nanofibers to perform single nanofiber experiments. Three-point bending tests for single suspended nanofibers over an AFM grid, and micro-structured substrates for Young's modulus obtaintion through a mechanical model and to determine boundary conditions.

From this Young's modulus of PVA and PVA/SG/Ch nanofibers was obtained as a characterization for scaffolds based in these polymeric fibers, allowing for a comparison between the scaffold itself as a material and the single fibers, presenting different stiffness, as we increase the scale, the mechanical modulus increases with the reduction of the scale, i.e, the mechanical modulus for electrospun mats is lower than the measured in nanofibers. Moreover, mechanical stiffness decreases as relative humidity increases in general, and as expected, Young's modulus is generally higher for the blended formulation of PVA/SG/Ch, with the exception of the nanofiber under high humidity, where the stiffness decreased at a faster rate than the PVA nanofiber.

The results obtained by the three-point bending method are promising for characterizing nanofibers mechanically, still it is necessary to enlarge the sample

size of nanofibers, to truly compare the variance of this method, as Young's moduli of some nanofibers yielded unusually large values, as high as $26GPa$. Also, the change in mechanical moduli with relative humidity for both nanofibers hinted a glass transition induced by humidity, which could explain the drastic drop in the mechanical modulus of the nanofibers at $60\%RH$ for PVA and around $30\%RH$ for the blend.

In future work, it is important to obtain a larger sample size of nanofibers for mechanical testing to determine if the three-point bending method can better describe the properties of nanofibers in comparison with the non-suspended fibers over silicon wafers. Study the breaking point of these nanofibers on the micro-structured grid with variable humidity to realize if the change in mechanical properties are related to a glassy to rubbery transition, and establish a temperature treatment for the polymeric solution, since in our measurements the temperature was not a variable that could be manipulated. However, it is pertinent to ask how the structure of these nanofibers change with humidity, temperature, and formulation, since the stiffness of the blended nanofibers decreases at lower humidities than the PVA ones.

Chapter 5

Master's products

As this Master's thesis was developed, some products were produced in various forms, like expositions in national and international conferences, an internship abroad, a participation in a published paper, and another participation in a submitted manuscript.

5.1 Congresses and conferences

1.- ITMR2023 (*Congreso Nacional de Ingeniería de Tejidos y Medicina Regenerativa*),poster "*Propiedades Higromecánicas a Multiescala de Nanofibras Electrohiladas de PVA/GS/QUI*". Benjamín Schleyer-Thiers, Sebastián Véliz, Catalina Navarrete, Catalina Montecino, Constanza Rodríguez, Dragica Bezjak, Cristian Acevedo, Tomas P. Corrales.

2.- CNN7(*Congreso Nacional de Nanotecnología VII*), poster "Multiscale Mechanical Properties of Elefctrospun mats based of PVA, Salmon Gelatin and Chitosan". Benjamín Schleyer-Thiers, Sebastián Véliz, Catalina Navarrete, Constanza Rodríguez, Martín Chavarría, Tomas P. Corrales.

3.- eNE2024(*XIII Escuela de Nanoestructuras*), talk "Hygromechanical properties: comparison between PVA and PVA/GS/QUI nanofibers". Benjamín Schleyer-Thiers, Sebastián Véliz, Dragica Bezjak, Tomas P. Corrales.

4.- International congress XXII B-MRS 2024 (Brazilian Materials Research Society meeting), talk "Three-point bending tests of single hygroscopic nanofibers and emergent mechanical properties on scaffolds". Benjamín Schleyer-Thiers, Dragica Bezjak, Tomas P. Corrales.

5.- "*XXIV Simposio Chileno de Física*", poster "Three-point bending tests of single hygroscopic nanofibers and emergent mechanical properties on scaffolds". Benjamín Schleyer-Thiers, Dragica Bezjak, Tomas P. Corrales.

6.- eNE2025(*XIII Escuela de Nanoestructuras*), talk "Hygromechanical properties of biopolymer based scaffolds, characterized through colloidal probe technique". Benjamín Schleyer-Thiers, Dragica Bezjak, Tomas P. Corrales.

5.2 Internship

Assisted to an abroad internship in Heidelberg University IMSEAM (Institute for Molecular System Engineering and Advanced Materials) Heidelberg, Germany during a month.

5.3 Papers

1.- Bravo, L., Ampuero, M., Correa-Puerta, J., Corrales, T. P., Flores, S., Schleyer, B., Hassan, N., Häberle, P., Henríquez, R., & del Campo, V. (2024). Glass Surface Nanostructuring by Soft Lithography and Chemical Etching. Nanomaterials, 14(21), 1714.
(https://doi.org/10.3390/nano14211714).

2.- "Blending Salmon Gelatin with Polyvinylidene fluoride using coaxial electrospinning" Martin Chavarria-Vidal, Dragica Bezjak, Benjamin Schleyer-Thiers, Maria Saavedra-Fredes, Tomas P. Corrales. BBA Advances. (In revision)

Bibliography

[1] A. Alessandrini and P. Facci. Afm: a versatile tool in biophysics. *Measurement science and technology*, 16(6):R65, 2005.

[2] M. Aslam, M. A. Kalyar, and Z. A. Raza. Polyvinyl alcohol: A review of research status and use of polyvinyl alcohol based nanocomposites. *Polymer Engineering & Science*, 58(12):2119–2132, 2018.

[3] B. I. P. Báez, C. A. M. Pérez, and E. S. Z. Aguilar. Fabricación de fibras poliméricas a base de pla obtenidas mediante electrohilado. *CULCyT: Cultura Científica y Tecnológica*, 17(1):2, 2020.

[4] M.-H. Bao. Basic mechanics of beam and diaphragm structures. In *Handbook of Sensors and Actuators*, volume 8, pages 23–88. Elsevier, 2000.

[5] G. Binnig and H. Rohrer. Scanning tunneling microscopy. *Surface science*, 126(1-3):236–244, 1983.

[6] G. Binnig, C. F. Quate, and C. Gerber. Atomic force microscope. *Physical review letters*, 56(9):930, 1986.

[7] R. Brown. *Handbook of polymer testing: physical methods*. CRC press, 1999.

[8] H.-J. Butt. A technique for measuring the force between a colloidal particle in water and a bubble. *Journal of Colloid and Interface Science*, 166(1): 109–117, 1994.

[9] H.-J. Butt, B. Cappella, and M. Kappl. Force measurements with the atomic force microscope: Technique, interpretation and applications. *Surface science reports*, 59(1-6):1–152, 2005.

[10] Y. Chen, B. L. Dorgan, D. N. McIlroy, and D. Eric Aston. On the importance of boundary conditions on nanomechanical bending behavior and elastic modulus determination of silver nanowires. *Journal of applied physics*, 100(10), 2006.

[11] A. C. Colorado, C. A. Agudelo, and M. E. Moncada. Análisis de biomateriales para uso en ingeniería de tejido de piel: revisión. *Revista Ingeniería Biomédica*, 7(14):11–23, 2013.

[12] T. P. Corrales, K. Friedemann, R. Fuchs, C. Roy, D. Crespy, and M. Kappl. Breaking nano-spaghetti: Bending and fracture tests of nanofibers. *Langmuir*, 32(5):1389–1395, 2016.

[13] E. S. Costa-Júnior, E. F. Barbosa-Stancioli, A. A. Mansur, W. L. Vasconcelos, and H. S. Mansur. Preparation and characterization of chitosan/poly (vinyl alcohol) chemically crosslinked blends for biomedical applications. *Carbohydrate polymers*, 76(3):472–481, 2009.

[14] E. Dintwa, E. Tijskens, and H. Ramon. On the accuracy of the hertz model to describe the normal contact of soft elastic spheres. *Granular Matter*, 10: 209–221, 2008.

[15] Y. M. Efremov, D. Bagrov, M. Kirpichnikov, and K. Shaitan. Application of the johnson–kendall–roberts model in afm-based mechanical measurements on cells and gel. *Colloids and Surfaces B: Biointerfaces*, 134:131–139, 2015.

[16] T. S. Gaaz, A. B. Sulong, M. N. Akhtar, A. A. H. Kadhum, A. B. Mohamad, and A. A. Al-Amiery. Properties and applications of polyvinyl alcohol, halloysite nanotubes and their nanocomposites. *Molecules*, 20(12):22833–22847, 2015.

[17] G. Guhados, W. Wan, and J. L. Hutter. Measurement of the elastic modulus of single bacterial cellulose fibers using atomic force microscopy. *Langmuir*, 21(14):6642–6646, 2005.

[18] P. Hansma, J. Cleveland, M. Radmacher, D. Walters, P. Hillner, M. Bezanilla, M. Fritz, D. Vie, H. Hansma, C. Prater, et al. Tapping mode atomic force microscopy in liquids. *Applied physics letters*, 64(13):1738–1740, 1994.

[19] H. Hu, X. Zhang, Y. He, Z.-s. Guo, J. Zhang, and Y. Song. Combined effect of relative humidity and temperature on dynamic viscoelastic properties and glass transition of poly (vinyl alcohol). *Journal of Applied Polymer Science*, 130(5):3161–3167, 2013.

[20] J. L. Hutter and J. Bechhoefer. Calibration of atomic-force microscope tips. *Review of scientific instruments*, 64(7):1868–1873, 1993.

[21] M. Kappl and H.-J. Butt. The colloidal probe technique and its application to adhesion force measurements. *Particle & Particle Systems Characterization: Measurement and Description of Particle Properties and Behavior in Powders and Other Disperse Systems*, 19(3):129–143, 2002.

[22] C. A. Karina Catalán, T. Corrales. Inhomogeneous nanofiber swelling measured with environmental afm. 2020.

[23] D. Kluge, F. Abraham, S. Schmidt, H.-W. Schmidt, and A. Fery. Nanomechanical properties of supramolecular self-assembled whiskers determined by afm force mapping. *Langmuir*, 26(5):3020–3023, 2010.

[24] W. Menacho, K. N. Catalan, T. P. Corrales, and H. V. Guzman. Quantitative dynamic afm hydration-adsorption design for hygroscopic and biocompatible polymeric nanofibers. *Small Structures*, 5(4):2300379, 2024.

[25] L. S. Nair and C. T. Laurencin. Biodegradable polymers as biomaterials. *Progress in polymer science*, 32(8-9):762–798, 2007.

[26] C. A. Putman, K. O. Van der Werf, B. G. De Grooth, N. F. Van Hulst, and J. Greve. Tapping mode atomic force microscopy in liquid. *Applied physics letters*, 64(18):2454–2456, 1994.

[27] Â. Semitela, A. F. Girão, C. Fernandes, G. Ramalho, I. Bdikin, A. Completo, and P. A. Marques. Electrospinning of bioactive polycaprolactone-gelatin nanofibres with increased pore size for cartilage tissue engineering applications. *Journal of Biomaterials Applications*, 35(4-5):471–484, 2020.

[28] D. serrato Ochoa, R. N. Aguilar, and A. A. Méndez. Ingeniería de tejidos. una nueva disciplina en medicina regenerativa tissue engineering. a new discipline in regenerative medicine.

[29] R. M. Soares, N. M. Siqueira, M. P. Prabhakaram, and S. Ramakrishna. Electrospinning and electrospray of bio-based and natural polymers for biomaterials development. *Materials Science and Engineering: C*, 92:969–982, 2018.

[30] T. T. Stanislas, K. Bilba, R. P. de Oliveira Santos, C. Onésippe-Potiron, H. Savastano Junior, and M.-A. Arsène. Nanocellulose-based membrane as a potential material for high performance biodegradable aerosol respirators for sars-cov-2 prevention: a review. *Cellulose*, 29(15):8001–8024, 2022.

[31] G. R. Strobl and G. R. Strobl. *The physics of polymers*, volume 2. Springer, 1997.

[32] M. I. Taborda, K. N. Catalan, N. Orellana, D. Bezjak, J. Enrione, C. A. Acevedo, and T. P. Corrales. Micropatterned nanofiber scaffolds of salmon gelatin, chitosan, and poly (vinyl alcohol) for muscle tissue engineering. *ACS omega*, 8(50):47883–47896, 2023.

[33] S. M. Tan, X. Y. Teoh, J. Le Hwang, Z. P. Khong, R. Sejare, A. Q. Almashhadani, R. Abou Assi, and S. Y. Chan. Electrospinning and its potential in fabricating pharmaceutical dosage form. *Journal of Drug Delivery Science and Technology*, 76:103761, 2022.

[34] W. E. Teo and S. Ramakrishna. A review on electrospinning design and nanofibre assemblies. *Nanotechnology*, 17(14):R89, 2006.

[35] T. E. ToolBox. Saturated salt solutions - controlling air humidity. Technical report, [online] Available at: https://www.engineeringtoolbox.com/salt-humidity-$d_1887.html[Accessed31-03-2025]$, 2014.

[36] S. Ullah, I. Zainol, S. R. Chowdhury, and M. Fauzi. Development of various composition multicomponent chitosan/fish collagen/glycerin 3d porous scaffolds: Effect on morphology, mechanical strength, biostability and cytocompatibility. *International journal of biological macromolecules*, 111:158–168, 2018.

[37] S. R. Vasco, C. A. V. Isaza, M. L. M. Suaza, J. Z. Giraldo, and M. E. M. Acevedo. *Ingeniería de tejidos y aplicaciones*. Instituto Tecnológico Metropolitano, 2016.

[38] A. Vats, N. Tolley, J. Polak, and J. Gough. Scaffolds and biomaterials for tissue engineering: a review of clinical applications. *Clinical Otolaryngology & Allied Sciences*, 28(3):165–172, 2003.

[39] C. Wei, T.-Q. Gang, L.-J. Chen, and Y. Zhao. Critical condition for the transformation from taylor cone to cone-jet. *Chinese Physics B*, 23(6):064702, 2014.

[40] A. L. Yarin, S. Koombhongse, and D. H. Reneker. Taylor cone and jetting from liquid droplets in electrospinning of nanofibers. *Journal of applied physics*, 90(9): 4836–4846, 2001.

[41] Y. Yin, Z. Pan, and J. Xiong. A tensile constitutive relationship and a finite element model of electrospun nanofibrous mats. *Nanomaterials*, 8(1):29, 2018.

[42] N. E. Zander. Hierarchically structured electrospun fibers. *Polymers*, 5(1):19–44, 2013.

[43] W. Zuo, M. Zhu, W. Yang, H. Yu, Y. Chen, and Y. Zhang. Experimental study on relationship between jet instability and formation of beaded fibers during electrospinning. *Polymer Engineering & Science*, 45(5):704–709, 2005.